UNIVERSITY OF OKLAHOMA

GRADUATE COLLEGE

THE FEASIBILITY OF USING X-RAY INDUCED ACOUSTIC COMPUTED TOMOGRAPHY FOR NON-DESTRUCTIVE TESTING OF AIRCRAFT STRUCTURAL

A THESIS

SUBMITTED TO THE GRADUATE FACULTY

in partial fulfillment of the requirements for the

Degree of

MASTER OF SCIENCE

By

TIFFANY TRAN
Norman, Oklahoma
2020

THE FEASIBILITY OF USING X-RAY INDUCED ACOUSTIC COMPUTED TOMOGRAPHY FOR NON-DESTRUCTIVE TESTING OF AIRCRAFT STRUCTURAL

A THESIS APPROVED FOR THE
SCHOOL OF AEROSPACE AND MECHANICAL ENGINEERING

BY THE COMMITTEE CONSISTING OF

Dr. Yingtao Liu, Chair

Dr. Liangzhong Xiang, Co-Chair

Dr. Jivtesh Garg

Acknowledgments

First of all, I would like to express my deep gratitude to my advisor, Dr. Yingtao Liu, for his support, enthusiasm, and guidance to complete this master thesis.

I would like to express my sincere thanks to Dr. Liangzhong Xiang, for the opportunity to join his lab, and for his enthusiastic guidance in the process of using the XACT technique.

I would also like to take this opportunity to thank Dr. Jivtesh Garg for serving as a member of my committee and for his valuable advice throughout the learning process.

Thank you to my mentor, Pratik Samant for your guidance on the process of learning the K-wave simulation and to all of my present and former colleagues for the motivation and collaboration.

Finally, I would like to thank my parents, Chi and Cuong, sisters, Vi and Uyen, and fiancé, Thomas, for their encouragement, support, and unconditional love.

Table of Contents

List of Figures

List of Tables

Abstract

Aviation safety is a very important aspect of the aviation industry. One of the most important methods for increasing aviation safety is the non-destructive testing method. The non-destructive testing method is considered to be the most effective method for checking defects, widely used in the aviation industry. X-ray induced Acoustic Computed Tomography (XACT) is a new novel imaging modality based on the X-ray induced acoustic effect. A short-pulsed of X-rays are required to achieve a thermal response and generate acoustic waves due to thermoelastic expansion. XACT takes advantage of X-ray absorption contrast with the ultrasonic spatial resolution for deep imaging. The goal of this work is to demonstrate the feasibility of XACT for defect detection in aircraft structures as a non-destructive testing method to overcome the limitations of most frequent techniques used non-destructive testing (NDT) methods are outlined in Chapter 1.

In this work, there are two main objectives to demonstrate the XACT technique are as follows, (1) introduce and proving the feasibility of XACT through simple models and (2) a full demonstration of XACT with three models from simple to complex structures. This work demonstrates that XACT has the potential to be implemented in-field NDT for aircraft maintenance and inspection due to its feasibility in detect defects with accessibility to a single side of the object.

Chapter 1: Introduction

1.1 Background of Nondestructive Testing

Non-destructive testing (NDT) methods are a technical discipline of inspection, quality diagnosis, and the integrity of structures by methods that do not harm the functionality of the test objects [1–6]. NDT is widely used in almost all industries, such as oil and gas, energy, shipbuilding, chemical, and food processing industries; especially in the aviation industry. Within the aviation industry, NDT is an indispensable tool for the maintenance and inspections of civil and military aircraft. NDT technologies can be used throughout the life of an aircraft, from determining the quality of aerospace materials to inspecting the performance and aircraft structures. Currently, non-destructive testing applications used on the airframe, structures, and landing gear account for about 80% inspection process [1,2,7].

NDT is also used to optimize the manufacturing processes of aircraft components. Early detection and removal of unsatisfactory components can optimize the manufacturing process [7–9]. In addition, timely detection of defects and damage in structures can help engineers devise remedial and repair options, avoiding possible aircraft disasters.

1.2 Overview of NDT Methods

NDT consists of many different methods and is divided into two groups accordingly to their ability in defect detection in aircraft inspections. For instance, Radiographic testing (RT) and ultrasonic testing (UT) methods are capable of detecting internal and surface defects. In contrast, visual testing (VT), liquid penetrant testing (PT), eddy-current testing (ECT), and magnetic particle inspection (MPI) are the methods used for the surface or

near-surface defects detection. The basic principles, advantages, and limitations of common NDT methods in aviation are outlined below.

1.2.1 Visual Testing – VT

This method is often overlooked in the list of NDT methods, visual inspection is one of the most popular and most effective in the sense of non-destructive testing in aircraft maintenance. The method is used to detect surface defects or structural damage for all materials [1,10]. Using optical instruments can check for internal defects and voids of internal structures, landing gears, etc. For visual inspection, the surface of the test object should have sufficient brightness and visibility of the inspector. For the inspection to be effective, the inspector needs to understand all the knowledge about the object to be inspected [11,12].

1.2.2 Liquid Penetrant Inspection – LPI

This is a method used to detect the discontinuities that unfold on the surface of materials of any industrial product made of non-porous materials of aircraft. The method is commonly used to test non-magnetic materials. In this method, a liquid penetrant is sprayed onto the surface of the product for a certain period so that the liquid penetrates the interior intermittently, and the residual absorbent is removed from the surface. The surface is then dried and covered with a developer substance. Absorbent substances that are contained in discontinuity and will be absorbed by the present substance to form an inspection indicator, reflecting the position and characteristics of the discontinuity [13–15].

The penetrant used in this method is visible dye and fluorescent absorbent. The dye penetrant is visible when performed under normal white light, while the fluorescent absorbent test is done under black light in darkroom conditions [16–18].

1.2.3 Eddy-current Testing - ECT

Eddy-current testing is a method used to detect defects on conductive materials, based on the effect of electromagnetic induction [20]. The principle of operation is when the alternating current (AC) flows through the coil, a changing magnetic field is created in the coil when the coil is placed near the conductor. The reciprocal magnetic field creates an eddy current in that conductor [21].

The eddy current in the conductor creates a pulsed magnetic field that opposes the original magnetic field. If there are any discontinuities on the conductor, it will affect the change of eddy current, as well as, change the magnetic field secondary coil that will record the change and generate a signal on the screen [21–24]. This method is very sensitive for detecting sub-surface cracks near the surface or corrosion of aircraft structures such as fasteners holes and bolt holes.

1.2.4 Magnetic Particle Inspection - MPI

Magnetic particle testing is one of the non-destructive testing methods (NDT) based on the principle of the magnetic field of the object to be tested and particles that react to electromagnetism [26]. This method can detect defects that open on the surface and immediately below the surface. Using an electromagnet to magnetize the object to be tested, then apply the magnetic powder to the surface of the object to be tested, the magnetic powder will rearrange according to the magnetic field lines in an orderly manner. The magnetic field lines will be deformed if there is a defect on the surface of the object.

It is a quick and effective test for detecting surface and subsurface defects in any shape. However, this method is only applicable to ferromagnetic materials and is widely used to test bolts, landing gear, gearboxes, shafts, etc. [22, 24–26].

1.2.5 Radiographic Testing – RT

The method uses X-ray tubes or radioactive sources to emit gamma rays through the object to be examined [1]. When passing through the object, the radiation beam weakens, the attenuation depends on the density of the material and the thickness that it passes through. When traveling through areas with defects, the intensity of the beam will be reduced less than when passing through areas without defects. These are the electromagnetic spectrum with very short wavelengths and very high energy. Gamma rays are often used to detect the internal structures and engines of an aircraft that require higher energy levels and parts are difficult to access [9, 27–31].

1.2.6 Ultrasonic Testing – UT

Ultrasound testing (UT) is one of the methods that can test metallic and non-metallic materials, high-frequency ultrasonic waves are transmitted into the test object. Ultrasonic testing is the most widely used method in the aviation industry to detect surface and subsurface defects of welds, forging, casting for undercarriage landing gear, engines, etc. Generally, this method is used with lots of different aircraft structures with very few limitations of materials [1,2,32].

Most ultrasonic testing methods are performed in a range of frequency 0.2 - 800 MHz. Ultrasonic waves propagate through the material and are accompanied by an attenuation by the properties of the material. The reflected sound waves are detected and analyzed in search of its defect and location. The degree of reflection depends greatly on the physical

state of the properties of the material and is partially reflected at the interface between metal - liquid or metal – solid [34–38].

1.2.7 Real-Time NDT: Structural Health Monitoring

In the last decade, the advancements of sensors and data analysis technologies have led to continuous on-board monitoring and real-time NDT of an engineering structure during operation, which is often referred to as Structural Health Monitoring (SHM) [39–41]. Integrated sensor systems including ultrasonic and thermographic equipment have been adopted for SHM applications [42–44]. In particular, acoustic and ultrasonic based SHM technologies are able to provide reliable detection of potential damage, allowing identification of damage locations and estimation of remaining useful lives of certain structures under given load conditions [45–48]. Furthermore, the most recent SHM technologies have allowed real-time structural health condition awareness under dynamic load conditions, such as fatigue and impact for various levels of structural scales including parts, components, and systems [49,50]. Potential environmental effects can also be considered during SHM analysis.

1.3 Summary of Advantages and Disadvantages of NDT Methods

The methods mentioned above have been beneficial in the non-destructive testing field, but some disadvantages need to be discussed. For instance, ultrasonic testing (UT) and methods for aircraft surface defects detection do not require access to both sides of the object compared to radiographic imaging methods. Yet, image reconstruction in RT offers high resolution with appropriate penetration depth. However, the disadvantage of RT is that the structural layers will overlap and may cause inaccuracies in locating defects. For internal defects detection and surface defects detection that involve radiation, there

is always a trade-off between depth of penetration and image resolution. However, the advantage of using surface defect detection techniques is that they only require access to one side of the object. Meanwhile, there is currently no method that can provide high resolution and increase depth detection with only accessibility of one side of the object and without going through many preparation steps.

Chapter 2: X-ray-induced Acoustic Computed Tomography and Its Applications

2.1 Background

2.1.1 Radiation-induced Acoustic Wave

Photoacoustic effect is a long-standing scientific discovery and was first observed by Alexander Graham Bell in 1880 using the sun as a source and human ears as sound signal detectors [51]. In the 1970s, with the advent of modern electronic devices, there was a renewed interest in this scientific technique. In 1983, a first experimental study of X-rays generated by synchrotrons was conducted. The researchers expect that intense X-rays are heat sources that can generate ultrasonic waves similarly to other heat sources. Here, photons have extremely short wavelengths that can penetrate through the object and generate ultrasonic waves. This research creates a new direction for objects where the laser cannot penetrate through some materials. Ultrasonic waves generated from X-rays are expected to give information about the internal properties of structures [52].

In 1991, the study was conducted to observe the sound waves generated from the edges of therapeutic X-rays with water absorbers and transducer, Bowen et al. [53]. The results obtained from the study demonstrate that acoustic signals can be generated from the edges of the X-ray beam in a medium of water. This application can accurately determine the position of the X-ray beam when delivering out to the important tissues that need to be treated, which can decrease the radiation dose. The study extends the application to patients being treated with therapeutic X-ray beams and other applications [53].

2.2 X-ray-induced Acoustic Computed Tomography (XACT) and Its Applications

2.2.1 Principle of XACT

The phenomenon of acoustic signals generated from X-ray was discovered in 1983, but until 2013, the first theoretical and experiments on XACT were proposed by Xiang et al. [41–44]. Since then, X-ray-induced computed tomography (XACT) has been implemented in various applications such as medical imaging, radiotherapy monitoring, and non-destructive testing of concrete infrastructure [45–48].

The principle of XACT is understood through the induction of the x-ray acoustic effect where x-rays are absorbed from the from inner-shell electrons during their excited state and therefore induce photoelectrons. The resulting atom then decays from one of two resulting processes; electromagnetic radiation or the Auger process. During these two processes, the kinetic energy that derives from the Auger electrons and photoelectron. This transfer in energy creates a thermal equilibrium from the increased number of collisions. Moreover, this transfer of energy from the atoms in thermal equilibrium to the atoms in the solid adheres to electron-phonon interactions [40, 49–51]. In turn, these interactions increase the thermal energy in the lattice itself. The x-ray acoustic generation and propagation is described by the following equation [50,52]:

$$\nabla^2 p(\boldsymbol{r}, t) - \frac{1}{v_s^2}\frac{\partial^2}{\partial t^2} p(\boldsymbol{r}, t) = -\frac{\beta}{C_p}\frac{\partial}{\partial t} H(\boldsymbol{r}, t) \tag{2.1}$$

Here, $p(\boldsymbol{r}, t)$ and $H(\boldsymbol{r}, t)$ denotes the acoustic pressure and heat source at position $\boldsymbol{r}$ and time t, respectively. β denotes the volumetric coefficient of thermal expansion, v_s denotes the speed of sound, and C_p denotes the specific heat capacity.

To generate a strong XA signal effectively, the two conditions are thermal confinement and the stress confinement must be met. The thermal confinement takes place when the

x-ray pulse is much shorter than the confinement time when the heat conduction is negligible during the excitation of the x-ray pulse. The condition can be expressed as [52,53]:

$$\tau < \tau_{th} = \frac{d_c^2}{4D_T} \tag{2.2}$$

Here, d_c denotes the spatial resolution and D_T denotes the thermal diffusivity of the object.

Stress confinement occurs when the x-ray pulse width is much shorter than the confinement time, where the pressure in an object needs to build up rapidly. The condition can be expressed as [52,53]:

$$\tau < \tau_{st} = \frac{d_c}{v_s} \tag{2.3}$$

Here, v_s denotes the speed of sound.

2.2.2 Biomedical Application

Since the XACT image was proposed and shown, XACT has been studied in various biomedical applications through many research groups around the world. The two applications in biomedical research that are most focused by researchers are therapeutic monitoring and diagnostic imaging. XACT's biomedical applications are tested with a variety of materials including lead, the chicken bone in the medium of water.

In diagnostic imaging, an experiment with the OU logo phantom aims to promote XACT technology/technique towards clinical practice [67]. To achieve that, an XACT system needs to be developed with the ability to provide images at a rapid rate with high resolution. Figure 2.1 illustrates the detail of an XACT system for the experiments. For the XACT imaging system, a ring array ultrasound transducer has 128 elements with a

center frequency of 5 MHz to achieve images with a spatial resolution of 138 μm. To receive the XA signal and store the XA signal effectively, a parallel data acquisition with a 128-channel pre-amplifier and 128-channel data acquisition module is used [67].

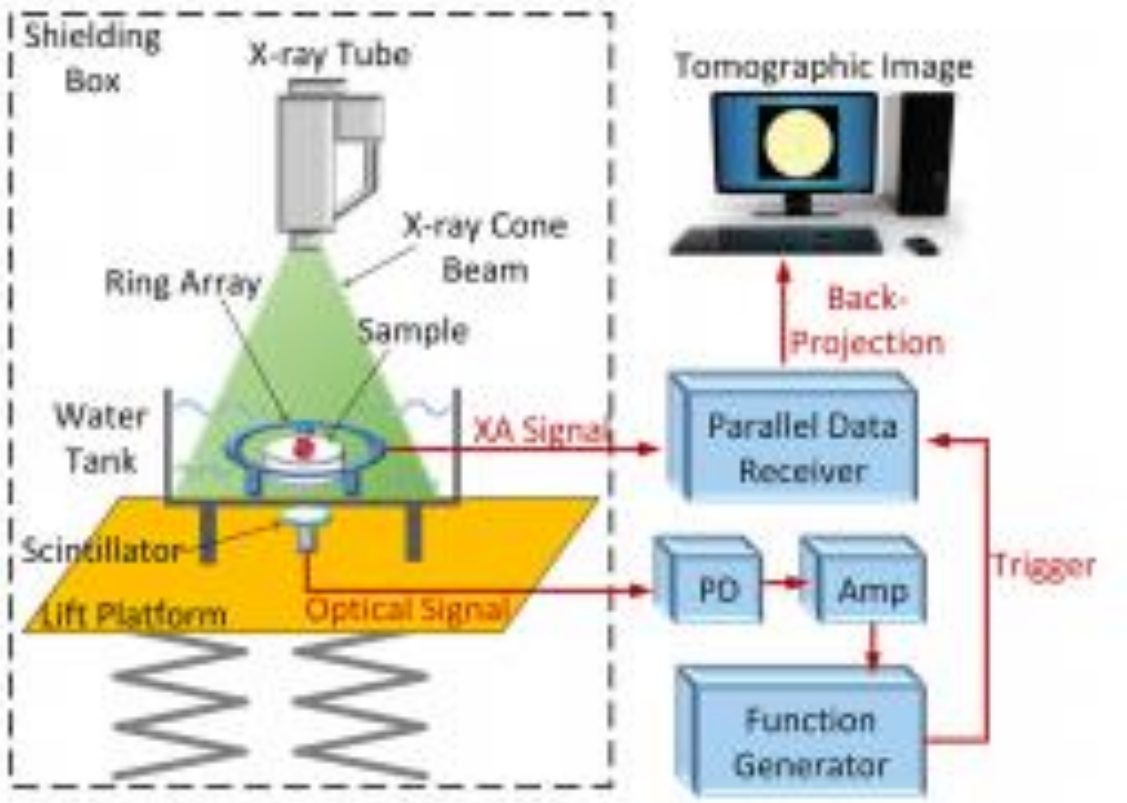

Figure 2.1. Schematic diagram of the XACT system for the OU logo phantom with an ultrasound transducer ring-array [67].

X-ray source features an ultra-short X-ray source with a pulse width of 60 ns, an exposure of 2.6 to 4.0 mR per pulse, and a pulse rate of 25 Hz. The OU logo is approximately 23 mm x 15 mm [67]. To reconstruct an XACT image, an average of 3800 times of XA data was collected, in Figure 2.2 results indicated the area of 30 mm x 30 mm. The results demonstrate that the imaging device and methodology provided the desired results, but there is an issue that needs to be discussed, and that is acoustic SNR is lower due to the fluency of X-rays decreases [67].

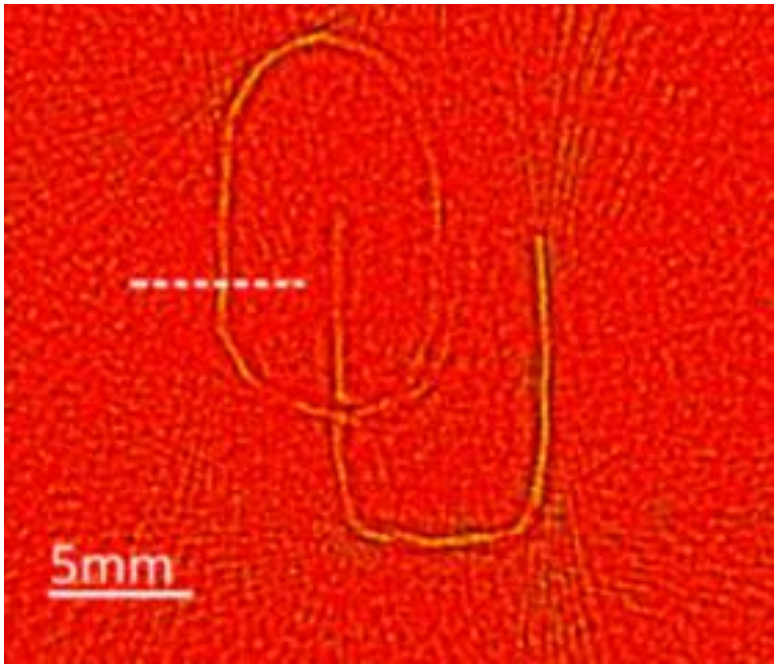

Figure 2.2. Reconstructed XACT image of the lead OU logo with the lead size of 150 μ [67].

For therapeutic monitoring, XACT imaging has been used in radiation oncology. Radiation therapy is one of the most common methods for treating cancer [68]. This method uses high-energy particles or waves such as X-rays, Gamma rays, electron beams, or protons to demolish and limit the growth of cancer cells. In radiotherapy, measurement of radiation dose should be done very carefully, errors in the calculation will likely cause serious injury and possibly death. Therefore, the demand for research in this field is increasing, the new method needs to be accurate, and the ability for real-time in vivo dosimetry [55,56]. An experiment was performed by irradiating a water tank with clinical radiation therapy using a LINAC to demonstrate the feasibility of XACT as a dosimetry tool [46,47]. Linac operates with pulse frequency at 120 Hz and provides 1.11 mGy each pulse at 2.4 cm to achieve maximum dose at depth. To detecting sound waves, a circular ultrasound probe with a center frequency of 0.5 MHz and 64% bandwidth [58]. The results obtained from the experimental to simulations demonstrate that the XACT image

has intensity related to the amount of radiation in an object with various sizes and shapes [58]. Additionally, proven that XACT has the potential in vivo dosimetry applications.

2.2.3 Non-destructive Testing for Concrete Infrastructure

The discussion of the basic principle of non-destructive testing along with the most common methods with the advantages and disadvantages are outlined in Chapter 1. In addition to biomedical applications, the XACT method is also extended to the non-destructive testing for concrete infrastructure [61]. A simulation study was conducted to demonstrate the feasibility of XACT in defects detection with three concrete samples of different sizes and shapes of defects. In addition, the XACT method only requires sing side accessibility of the object Figure 2.3, compared to the certain methods currently being applied to concrete, requiring both sides accessibility of the object. In the simulation study, XACT is used on small to large scale concrete. For a small-scale concrete application, the sub pavement model with the size of 30 by 30 cm was used, two defects with different sizes were placed 15 cm deep and 20 cm deep. As expected, Figure 2.4 defects can be easily detected through a reconstructed XACT image. A demonstration of XACT on a large scale of a 1m diameter bridge was performed. In Figure 2.5, reconstructed XACT image with a defect begun to display at the 0.45 m deep due to the blurred edges of the defect [61]. The results obtained from simulation studies using XACT to detect defects in concrete open up a new turning point for non-destructive testing applications.

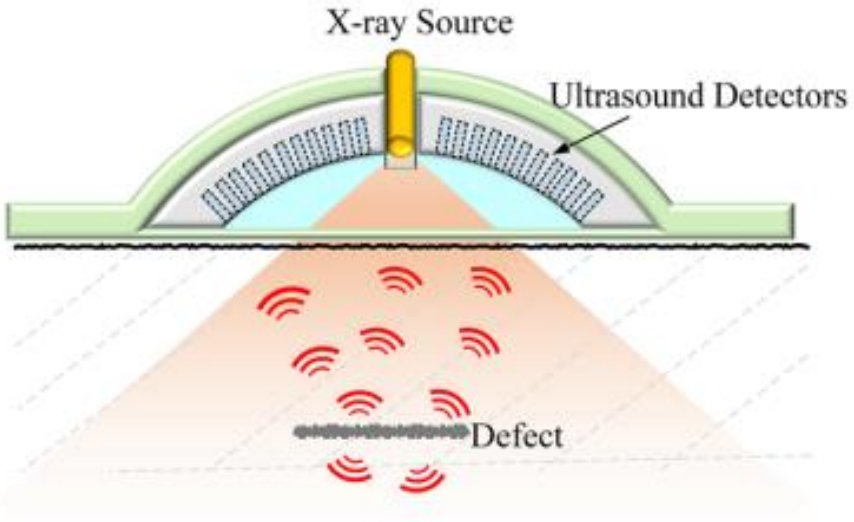

Figure 2.3. A schematic diagram of the proposal of XACT system for concrete infrastructure [61].

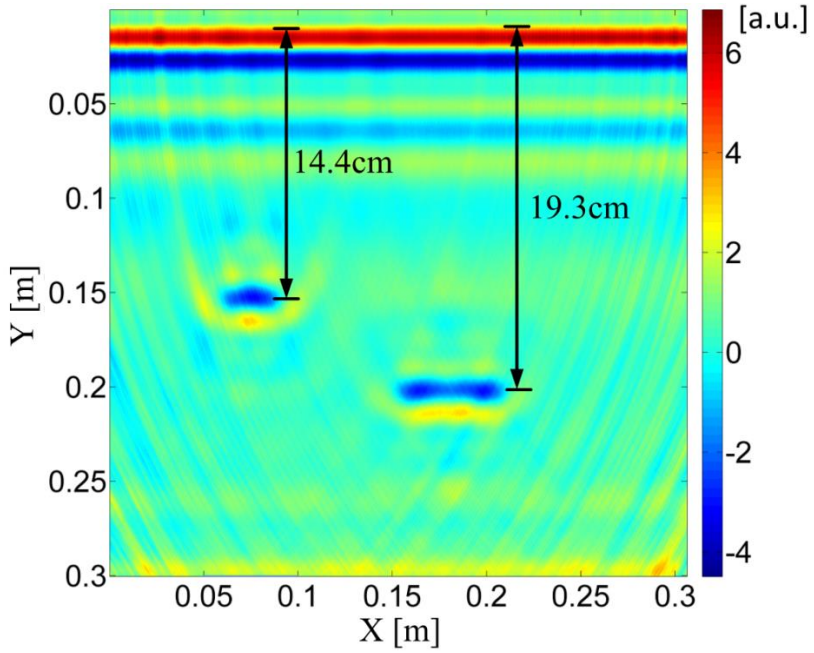

Figure 2.4. A reconstructed XACT image of sub-pavement concrete [61].

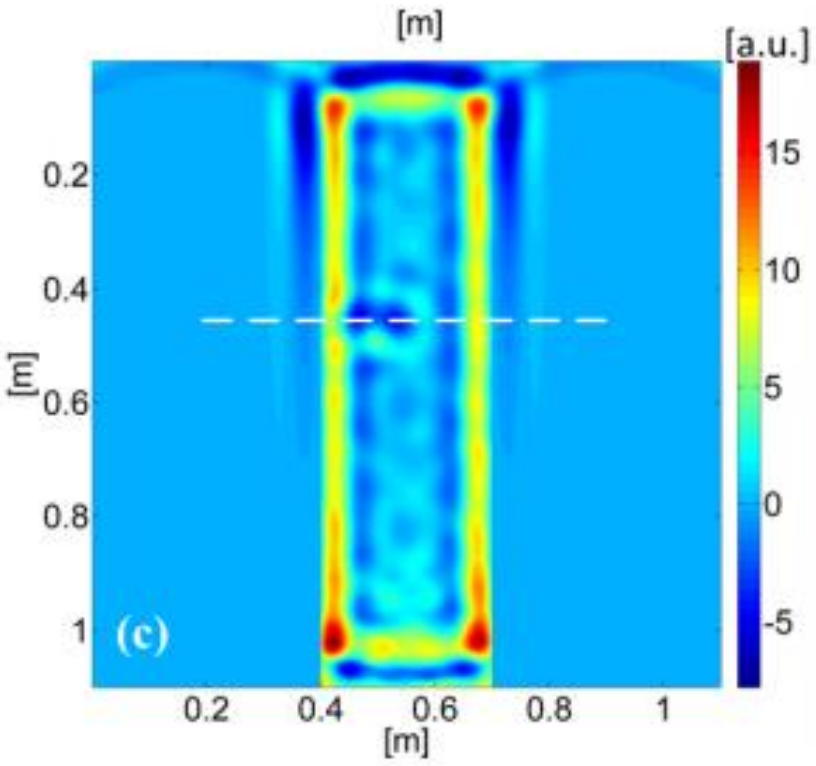

Figure 2.5. A reconstructed XACT image of a 1 m diameter concrete with a defect at 0.45 m deep [61].

2.3 Thesis motivation, objectives, and outline

The goal of this work is to demonstrate the feasibility of using XACT as a non-destructive testing method and to identify defects in aircraft structure to overcome the limitations of the current method discussed in Chapter 1. Hence, XACT imaging provides a high resolution from the X-ray absorption contrast and ultrasonic spatial resolution to increase the detection depth with the accessibility of a single side of the object. The two main objectives of this thesis are as follows, (1) introduce and proving the feasibility of XACT imaging in defect detection and (2) continue the demonstration with practical models and applicable parameters with multiple aircraft structures.

In the current aircraft's fuselage inspection, there are many tasks listed in the FAA class D [70]. However; the significant ones consist of a rigorous break down of the aircraft's

components in a systematic order. This includes sectioned portions of the fuselage along with the individual assembly components such as pressurized lines, as well as, conduits. The cockpit undergoes a similar inspection with a visual inspection of the throttle assembly and likewise, measurement instruments. Finally, the planes' exterior integrity is examined through a thorough removal of the wear-resistant paint to examine the external portion of the fuselage, as well as, rivets and other assembly parts. The maintenance of commercial aircraft will take place every 6 years and extremely thoroughly. The process can take a few months to complete and cost up to millions of US dollars. Therefore, the new method needs to have the potential to reduce time, cost, and generally improve the quality of testing for aircraft's fuselage [70].

In aircraft components, the landing gear is an important system during takeoff and landing. Landing gear plays a very important role and some of the common causes of failures are related to improper repair or maintenance. Similarly, to fuselage testing, various processes needs to be completed to achieve an effective test. However, cracks and corrosion in parts of the landing gear are difficult to detect due to the grease depositing on the surface. The areas inside the axes very susceptible to corrosion due to the water can get clogged, especially difficult to detect due to inaccessibility [58,59]. Therefore, NDT methods are usually performed, although often time it is impossible to verify whether there are defects or not.

To the best of our knowledge, this is the first research study to demonstrate the feasibility of XACT in defects detection capability in various aircraft structures. Chapter 3 of this thesis outlines the method and materials used for the simulation study in this work, while chapter 4 outlines the discussion and suggestion for future works.

Chapter 3: X-ray-induced Acoustic Computed Tomography for Aircraft Structures

3.1 Theory

3.1.1 Generation and propagation of acoustic pressure waves

Thermal expansion takes place as the temperature rises and creates acoustic waves due to vibrations of an atom and thus, will propagate in all directions. The acoustics waves will then be collected by the ultrasound transducer and reconstruct a 3-dimensional XACT image with a single projection, depending on the ultrasonic transducers. Figure 3.1 illustrates the proposal of the XACT inspection system for aviation structures. In x-ray scanning, the absorption of photons is reliant on the density of the materials whereas high-density materials will absorb photons more efficiently than that of low-density materials [73]. The X-ray induced acoustic initial pressure rises p_0 in the object can be expressed as [48,50],

$$p_0 = \Gamma \eta_{th} \mu F \tag{3.1}$$

Here, Γ is the dimensionless Grüneisen parameter, η_{th} represents the percentage of the energy absorbed in the object that is converted into heat and μ is the linear attenuation coefficient.

We define the dimensionless Grüneisen parameter as [63],

$$\Gamma = \frac{\beta}{\kappa \rho C_V} = \frac{\beta v_2^2}{C_p} \tag{3.2}$$

The fraction of an X-rays beam that is absorbed per unit thickness of the object is defined as [63],

$$\mu = \mu_a \rho \tag{3.3}$$

Here, μ_a denotes the X-ray mass attenuation absorption coefficient and ρ denotes the density of the material. F is the fluence, the intensity of the X-ray as it travels further away from the X-ray source at a given position is defined as [61],

$$F = \frac{n \,.\, E \,.\, C}{A} e^{-\mu x} \tag{3.4}$$

Here, n is the number of X-ray photons per pulse of 10^9, E is the X-ray energy, C is the charge of an electron of $1.6 \times 10^{-19}\, J/eV$, and A are the areas of the X-ray beam and x is the thickness of the object.

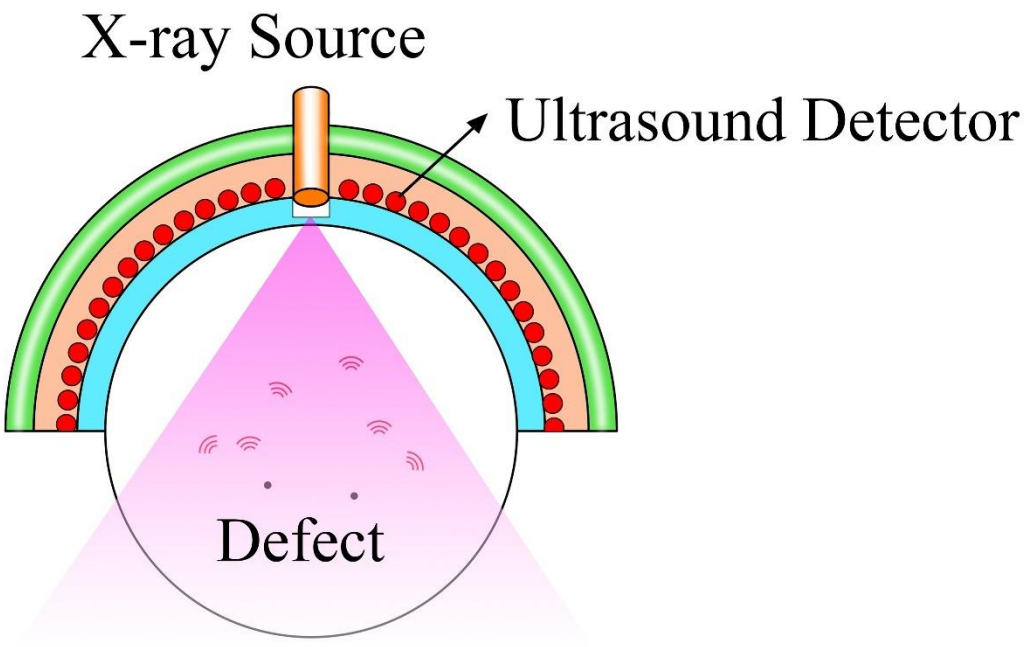

Figure 3.1. A schematic diagram of the XACT inspection system for aviation structures, the aircraft landing gear is shown in this figure.

3.1.2 Image reconstruction

In XACT imaging, there are three common techniques for image reconstruction: the fast Fourier transform algorithm, filtered back projection, and time reversal reconstruction. The combination of ultrasound detectors and algorithms is critical for a successful operation of reconstructing XACT image.

Time reversal algorithms are commonly used in a variety of applications, especially in PAI when the physical properties of the wave propagation remain unchanged when time is reversed and its flexibility. Time reversal technique based on the reciprocity equation [61–63]. In this work, reconstruction of the image was performed using a time-reversal algorithm for each of the models by using the MATLAB k-Wave toolbox [64,65].

3.2 Proof of XACT concept for aircraft stringer

A two-dimensional model was created in SolidWorks, with the length and width of the base plate is 10 inches, the thickness is 0.78 (39/50) inches and the distance between each of the stiffeners is 3.5 inches Figure 3.2. The initial pressure signal rise was calculated using the material properties listed in Table 1. for each of the simulations outlined in 3.1.1.

Table 1. Thermal acoustic parameters for Aluminum 6065, Inconel 625, and Defect

Parameters	**Aluminum 6065**	**Titanium 625**	**Defect**
Speed of Sound ($\boldsymbol{m/s}$)	6320	5820	1498
Density ($\boldsymbol{kg/m^3}$)	2800	8440	1000
Grüneisen parameters	1.34	1.9	0.12
Center Frequency ($\boldsymbol{MHz}$)	5		
Bandwidth (%)	75		

3.2.1 Simulation Setup and Results

The purpose of this study is to prove the feasibility of XACT in defect detection for metallic materials, therefore, we will use a circular array transducer with a total of 256 circular ultrasound detector elements equally spaced around of airplane's stiffener as shown in Figure 3.2. For our simulation study, four simulation models are developed using a two-dimensional image of an aircraft stiffener as an input image. The simulation setup for the studies performed is slightly different due to the defect shapes, size, and the properties of materials. In our simulation study, it is important to add frequency, as well as, to add noise to make the study as practical as possible. Therefore, the frequency of 5 MHz is added to the center ultrasound transducer with a bandwidth of 75%. In reconstructing the image, the value of the signal to noise ratio (SNR) of 40 dB is added to the recorded sensor data. The values of the X-ray mass attenuation coefficient are based on given energy, we choose the calculated values that will give the best imaging depth with the strongest signal.

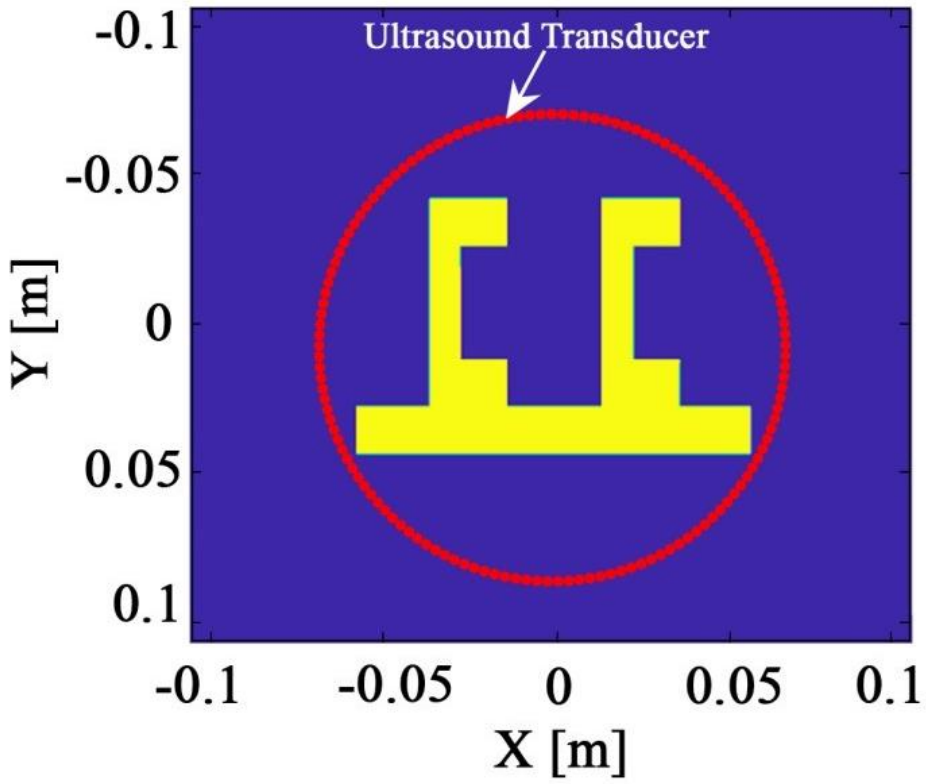

Figure 3.2. Illustrates the simulation setup with an aircraft's stiffener for all the for objective 1.

A demonstration to show the ability of XACT in the detection of voids caused during the fabrication process in Aluminum 6065, we created eight voids with sizes ranging from 0.5 mm to 3 mm arbitrary propagated in the base plate. The energy and the X-ray mass attenuation coefficient with the values of 50 KeV, $1.84 \times 10 - 1\ cm^2/g$, and $4.22 \times 10 - 2\ cm^2/g$ for Aluminum 6065 and defect, respectively. The properties of water are used in our simulation study as a defect in Figure 3.3.

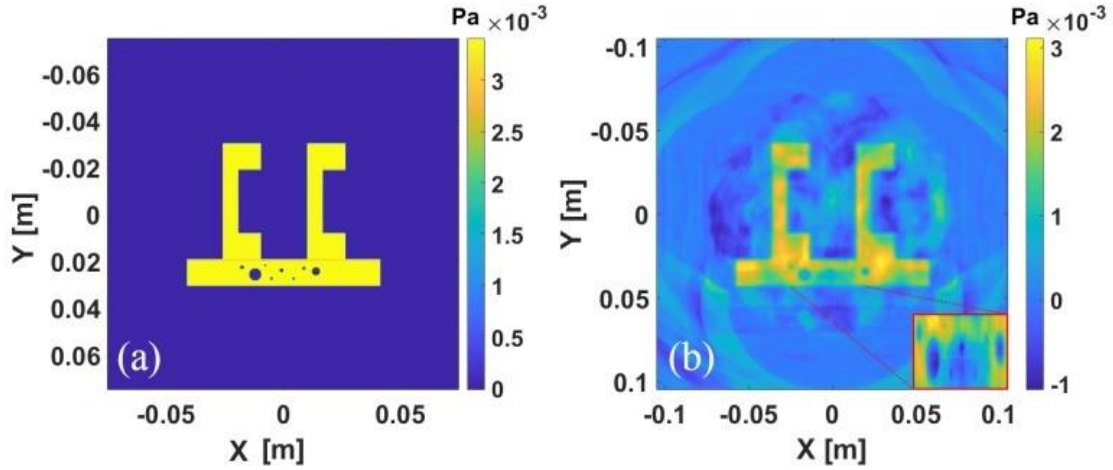

Figure 3.3. Simulation study for Aluminum 6065 with voids using XACT. (a) shows the initial pressure rise with the X-ray acoustic pressure generated throughout the entire plate. (b) shows the XACT reconstructed image zoomed in to the region with embedded voids.

A demonstration to show the ability of XACT in defect detection with a different shape due to impact damage in Aluminum 6065. A notch with a triangle shape on the surface of the aircraft's stiffener, with a base of 0.15 cm, and height is 0.17 cm in Figure 3.4.

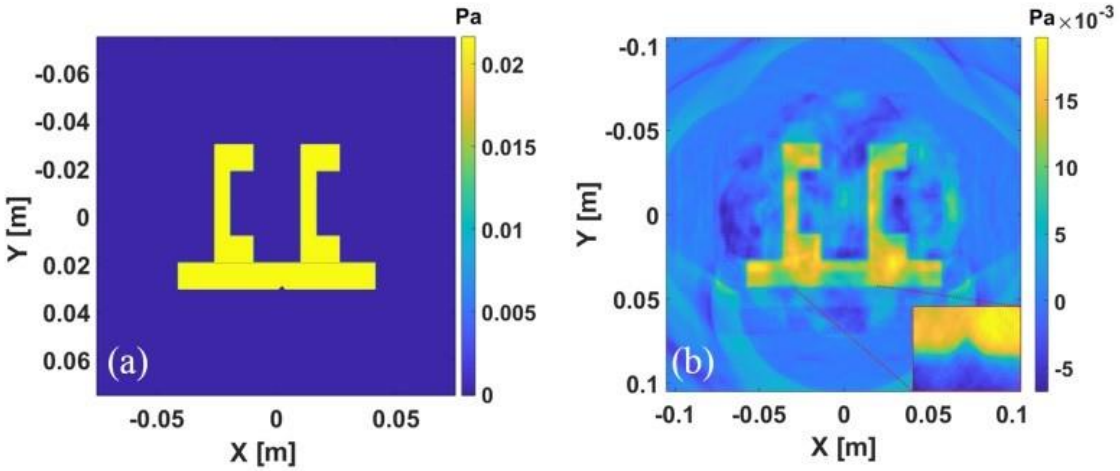

Figure 3.4. Simulation study for Aluminum 6065 with a notch using XACT. (a) shows the initial pressure rise with the X-ray acoustic pressure generated throughout the entire plate. (b) shows the XACT reconstructed image zoomed in at the interest region.

In XACT, due to the pressure is proportional to X-ray absorption and the dense materials tend to absorb more photons. The material is selected for these simulations is Inconel 625 to study the effects of energy on the ability of XACT in defect detection. Inconel 625 is

one of the materials mostly used for aircraft engines due to its resistance to high temperatures. We created a notch with a triangle shape on the surface of the aircraft's stiffener with a base of 0.15 cm, and height is 0.17 cm in Figure 3.5. Similarly, a demonstration with a defect of the shape of a triangle shown in Figure 3.6. The energy and the X-ray mass attenuation coefficient have the values of 50 KeV, $2.08\ cm^2/g$, and $2.97 \times 10^{-2} cm^2/g$ for Inconel 625 and defect, respectively. As you can see, the reconstructed image for Inconel 625 is slightly more visually obscured as compared to Aluminum 6065, the issue can be improved by increasing the energy of the X-ray sources.

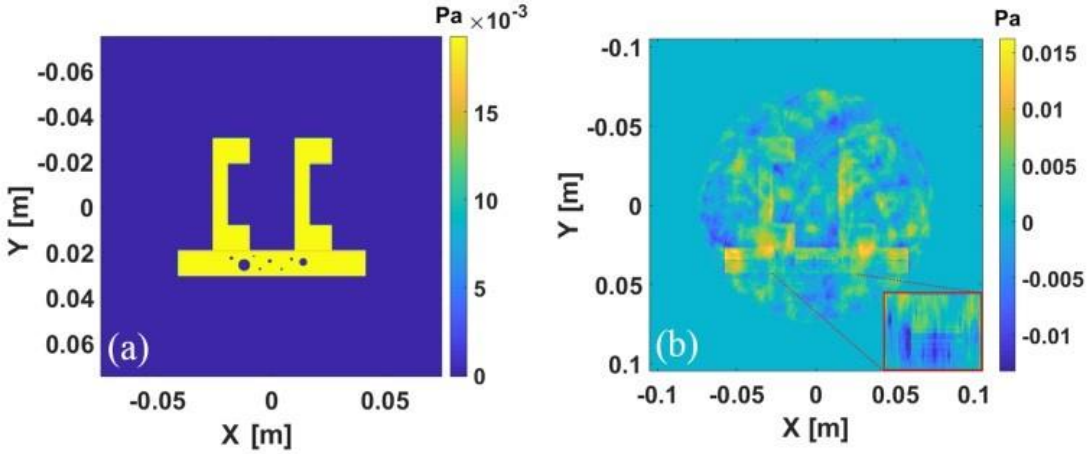

Figure 3.5. Simulation study for Inconel 625 with voids using XACT. (a) shows the initial pressure rise with the X-ray acoustic pressure generated throughout the entire plate. (b) shows the XACT reconstructed image zoomed in to the region with embedded voids.

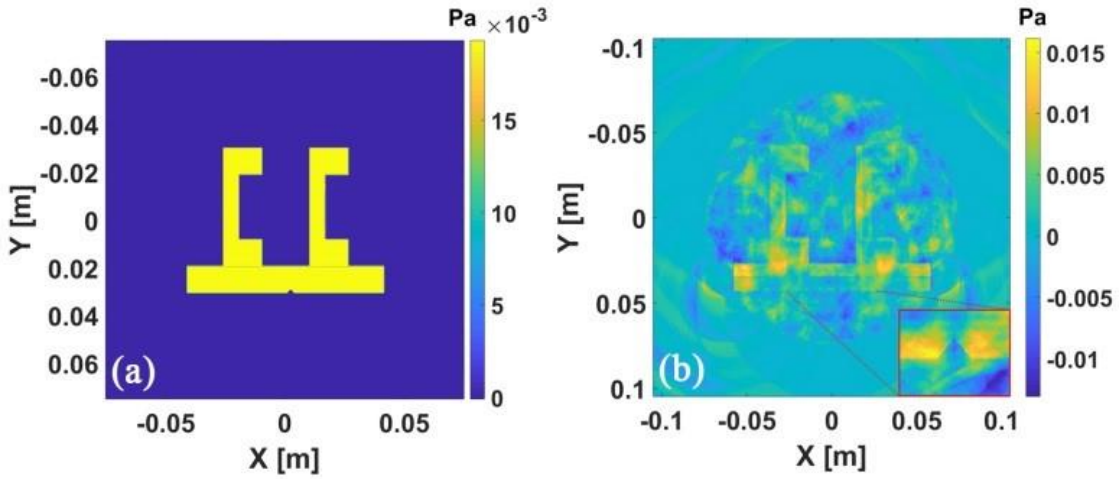

Figure 3.6. Simulation study for Inconel 625 with a notch using XACT. (a) shows the initial pressure rise with the X-ray acoustic pressure generated throughout the entire plate. (b) shows the XACT reconstructed image zoomed in to the region of interest.

3.3 A full demonstration of XACT imaging for aircraft structures

Since the results outlined in section 3.2.1 demonstrate the ability of XACT in defects detection, circular arrays transducer is not ideal for large-scale aircraft structures. The study for objective 2 will use the appropriate ultrasound frequencies, X-rays energies, and parameters used for each of the models.

3.3.1 Determination of Simulation Models

Three different models are created using SolidWorks and CAD software featuring of (1) a model of a skin-stiffener of aircraft fuselage Figure 3.7, (2) a model of a cylinder of landing gear with a diameter of 38.1 cm Figure 3.8, and (3) a model of aircraft panels with two different metallic materials secured by a rivet Figure 3.9. Models are designed to demonstrate the ability of XACT capability in defects detections with one-sided access from small scale to larger-scale complex aircraft structures. The initial X-ray induced acoustic (XA) was calculated using the thermal acoustic parameters of materials listed in Table 2 using equation 3.1

Table 2. Thermal acoustic parameters for Aluminum, Copper, Titanium, Zinc, and Defect

Parameters	***Aluminum***	***Zinc***	***Titanium***	***Defect***
Thermal Expansion $(\mathbf{10^{-6}K^{-1}})$	69	89.3	26	207
Speed of Sound $(\boldsymbol{m/s})$	6420	4210	6070	1498
Heat Capacity $(\boldsymbol{J/kg \cdot K})$	921.096	376.14496	544.284	4179.6
Density $(\boldsymbol{kg/m^3})$	2712	7480	4500	1000

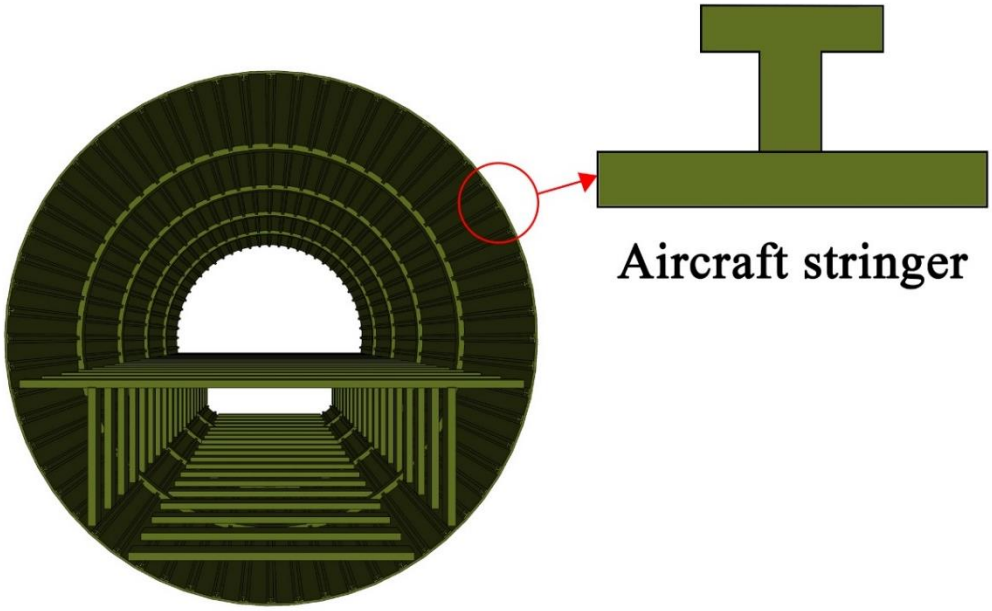

Figure 3.7. A model of aircraft fuselage shows a zoomed view of a single skin stiffener, with a base of 10 cm and a height of 3 cm.

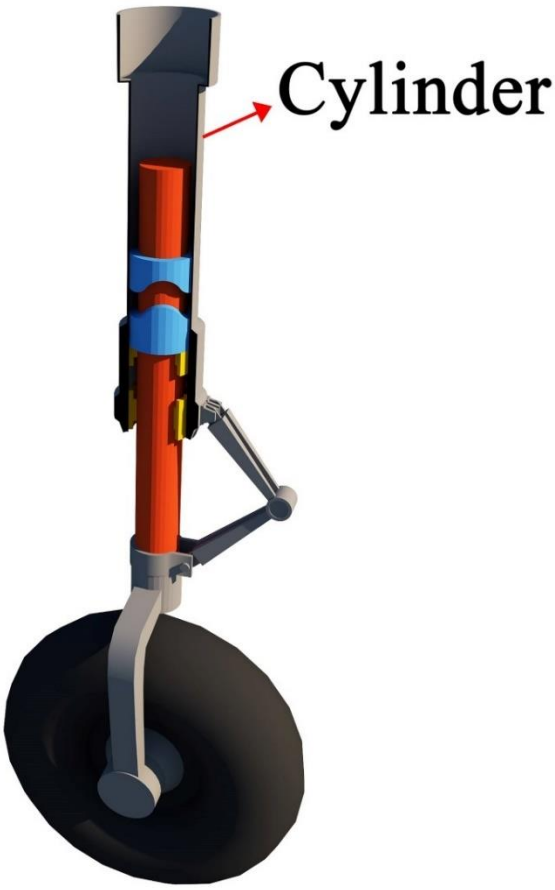

Figure 3.8. A model of aircraft landing gear with point out of a landing gear's cylinder.

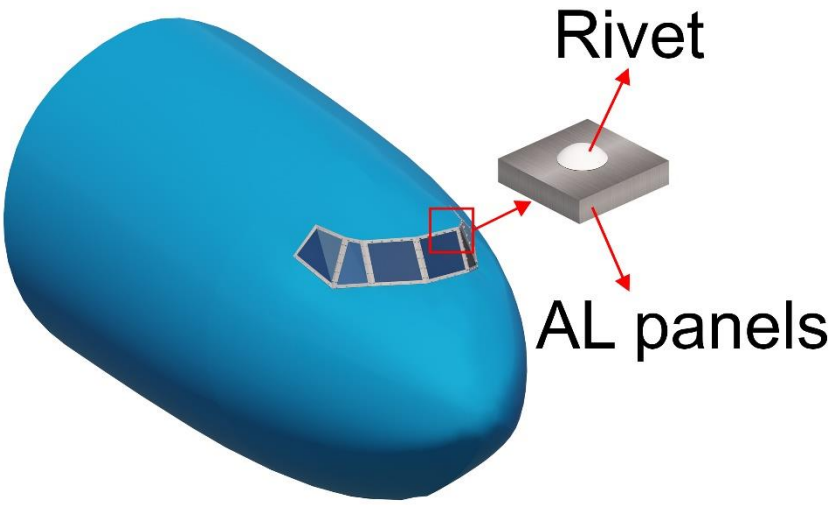

Figure 3.9. A model of aircraft panels with rivets used for fastening or joining alloys in aircraft construction or repair, a zoomed view with a size of 30 mm wide and thickness of 4 mm.

3.3.2 Determination for X-ray energy and ultrasound frequency

To demonstrate the XACT technique effectively, several factors such as the excitation pulse length, frequency, and transducer bandwidth need to be determined accordingly [66,67]. The level of ultrasonic attenuation is different due to the different ultrasonic absorption coefficient for each component of the object. In addition, the attenuation of ultrasound depends on the temperature of the object and the frequency of the ultrasonic beam. The higher the frequency then the faster the level of the attenuation, the depth of penetration will be less. In order to improve the penetration depth, it is necessary to reduce the frequency of the source or increase the energy of the ultrasound beam. In image methods, the trade-off between penetration depth and image resolution always exists.

However, the ultrasonic intensity at certain penetration depths can be calculated by [81]:

$$p = p_0 \cdot \alpha \cdot f \cdot z \tag{3.4}$$

Here, f is the ultrasound center frequency of the ultrasound decreases by 10% of the original intensity, z is the penetration depth, and $\alpha\ (dB/m/MHz)$ is the acoustic attenuation coefficient for aluminum, titanium and stainless steel with the values of 3.1, 14.5 and 9.9, respectively [69–71].

A spatial resolution can be calculated using [80]:

$$\Delta x = \frac{v_s}{f} \tag{3.5}$$

Here, Δx is the spatial resolution, v_s is the speed of sound, and f is the maximum frequency.

X-ray energy at certain penetration depths can be calculated by the following:

$$E_1 = n \cdot E \cdot e^{-\mu_a \rho x} \tag{3.6}$$

Here, E_1 denotes the X-ray energy decreases by 10% of the original energy E. A graph showing penetration depths as a function of ultrasonic frequency and X-ray energy for materials are displayed. As seen in Figure 3.10, 20 KeV X-rays and 1 MHz ultrasound can penetrate approximately 27 mm to 32 mm in Aluminum. Meanwhile, in Figure 3.11, 100 KeV X-rays and 20 kHz ultrasound can penetrate approximately 344 mm to 390 mm in Titanium. In Figure 3.12, 30 KeV X-rays and 2.5 MHz ultrasound can penetrate to 4 mm in Stainless Steel.

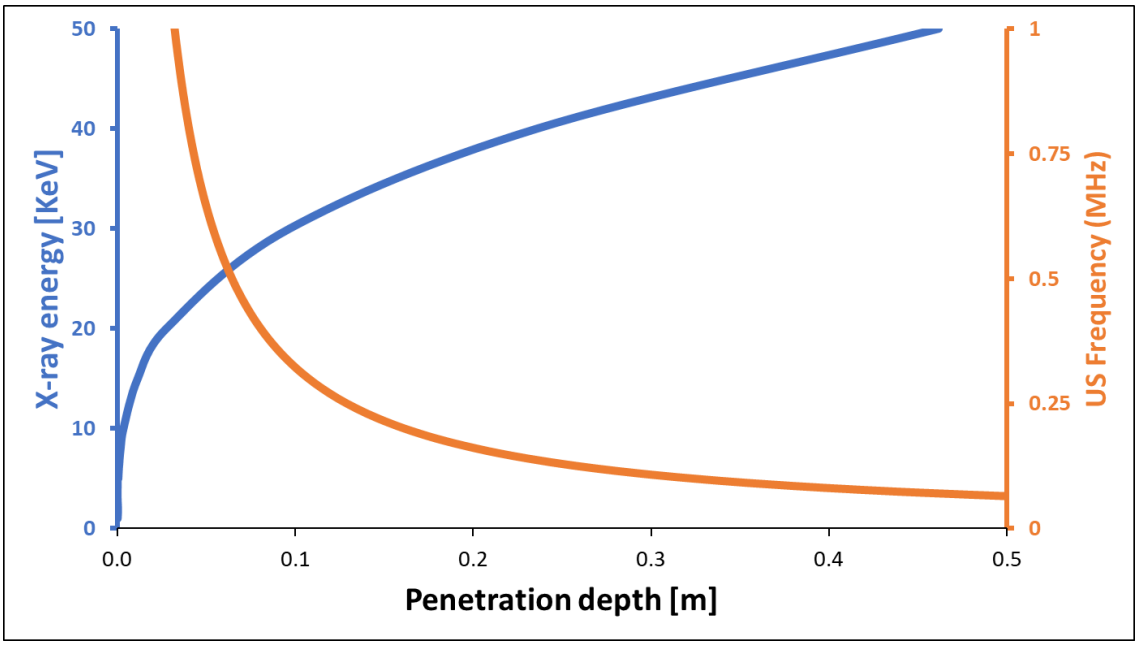

Figure 3.10. Penetration depth as a function of ultrasound frequency (orange) and penetration depth as a function of X-ray energy (blue) in Aluminum.

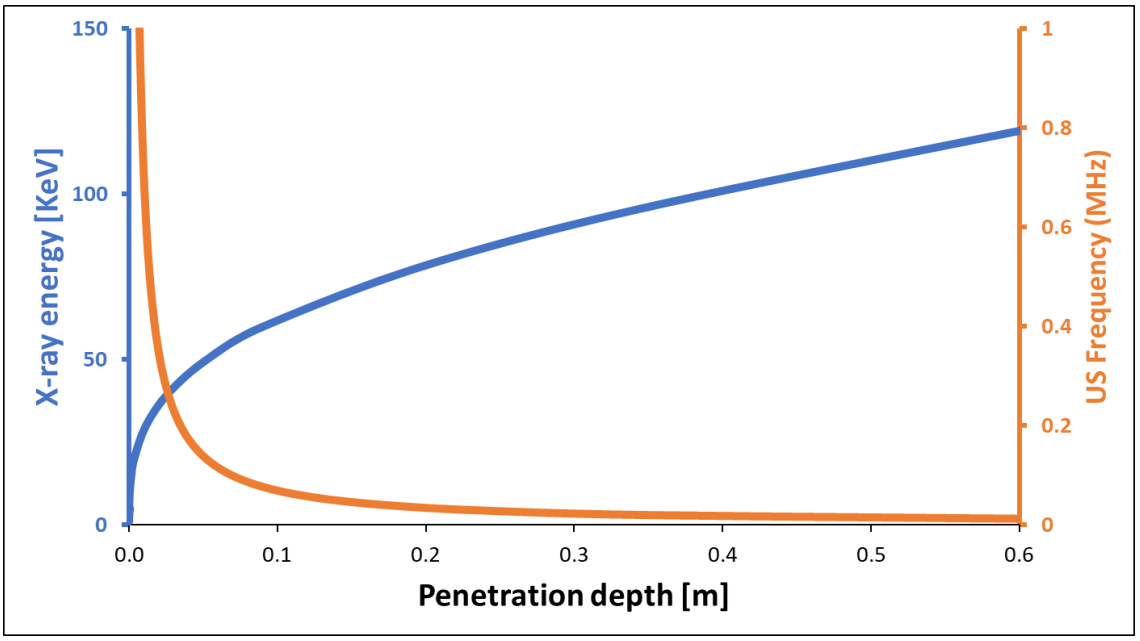

Figure 3.11. Penetration depth as a function of ultrasound frequency (orange) and penetration depth as a function of X-ray energy (blue) in Titanium.

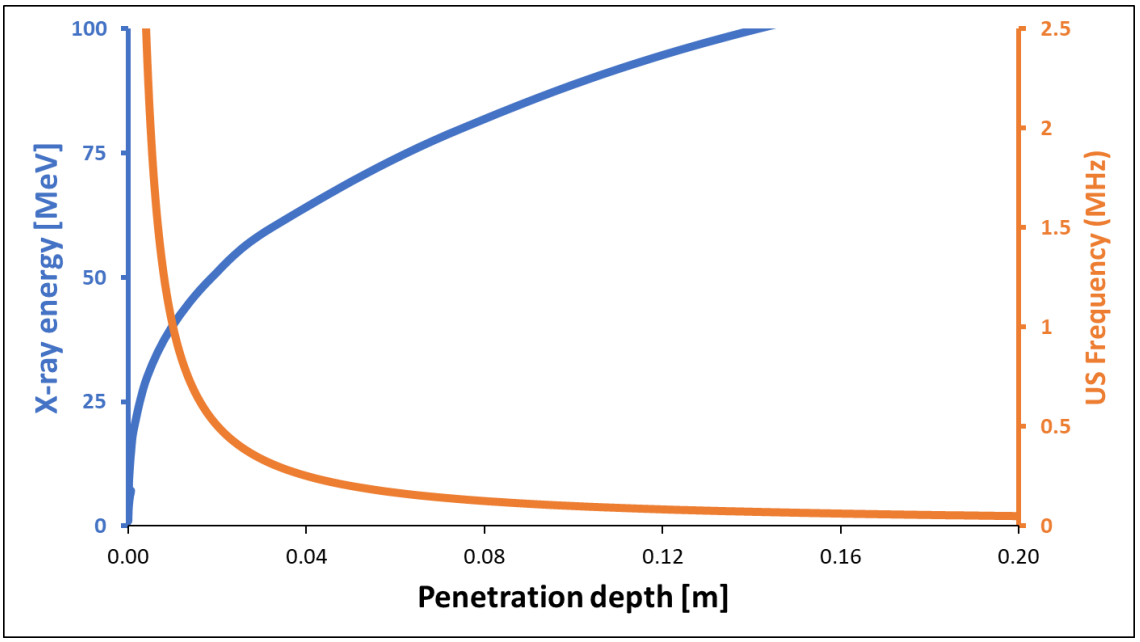

Figure 3.12. Penetration depth as a function of ultrasound frequency (orange) and penetration depth as a function of X-ray energy (blue) in Stainless Steel.

3.3.3 Simulations Setup and Results

Model 1: *An aircraft structural panel of the skin-stiffener*

To demonstrate the feasibility of the XACT technique in detecting cracks on the surface of the internal fuselage skin and skin-stiffener. A model of a single aircraft skin-stiffener was used in this simulation in Figure 3.7. In aircraft construction, stiffeners are used to support the skin carrying the load and to prevent bending under compression or shear loads. The stiffeners are fastened to the frames of the fuselage in the longitudinal direction of the aircraft, as seen in Figure 3.7 [72,73]. A triangle was created to represent the shape of a notch with a base of 100 μm and a height of 2 mm. Figure 3.13 illustrates the layout for the simulation, using linear X-ray arrays with a width of 10 cm and a beam thickness of 3 cm. In this model, a linear array ultrasound detector with 128 elements is evenly spaced on the surface of an aircraft fuselage. To collect XA signals, the center frequency of the 1 MHz ultrasonic detectors and 100% bandwidth were used in this model.

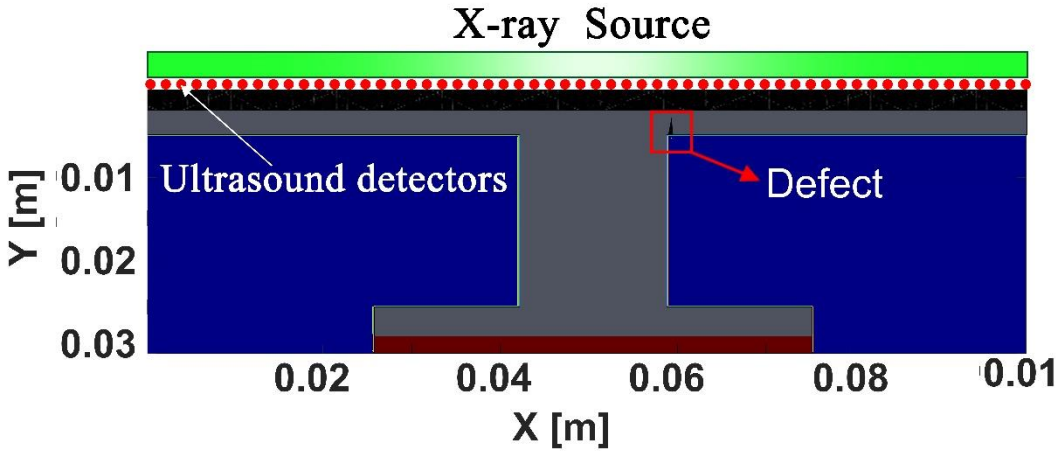

Figure 3.13. The model for defect detection with the linear X-ray source in green and ultrasound detectors in red is placed on the aircraft fuselage skin. The defect is created between the stringer and the fuselage skin in the red box.

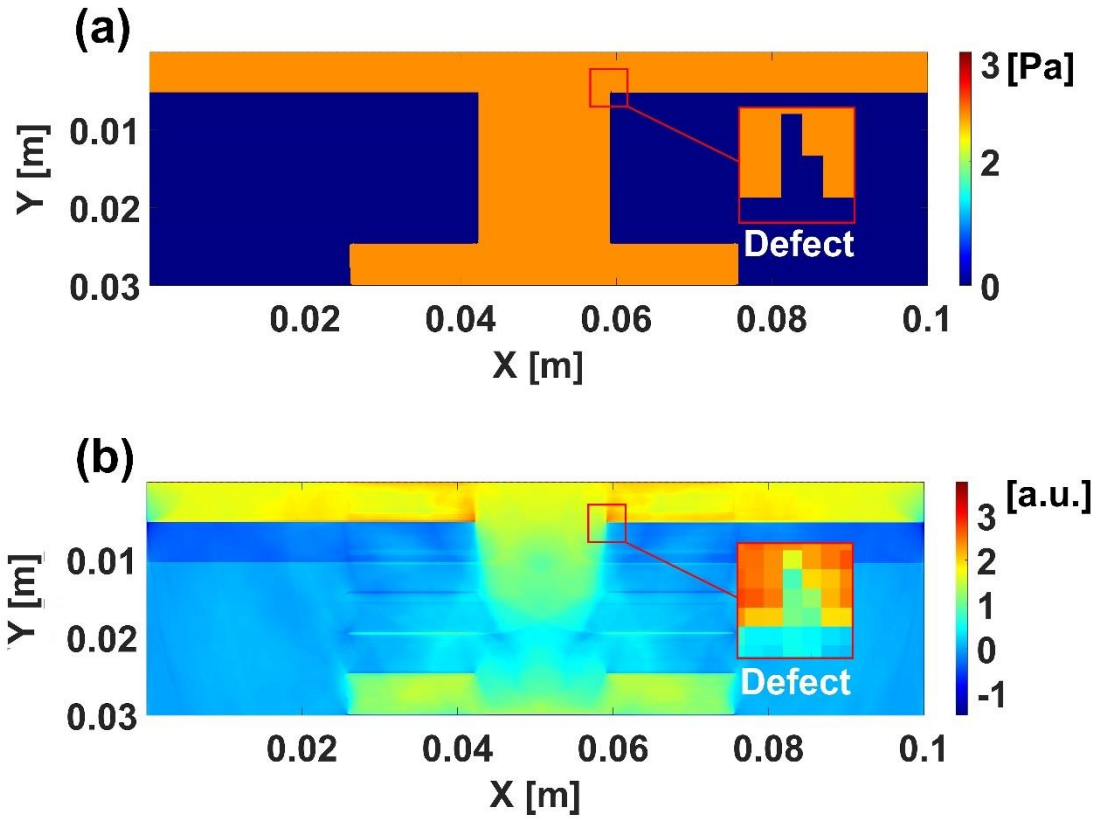

Figure 3.14. Defect detection and localization on the skin-stiffener using XACT (a) Initial XA pressure rise in the model with a zoomed view of the defect in the red square (b) Reconstructed XACT images with a zoomed view of the defect.

In Figure 3.14(a) shows an increase in the initial pressure XA with the energy used is 20 KeV. XA signals are collected by ultrasound detectors and are used to reconstruct XACT images in Figure 3.14(b). XACT can locate the position of the defect without accessing both sides of the large object, such as the entire aircraft fuselage. The location and shape of the defect match well with Figure 3.14(a). Although a defect is placed on the fuselage skin with a thickness of 5 mm, the X-ray energy of 20 KeV and ultrasound frequency of 1 MHz is used to penetrate approximately 30 cm deep, and results in imaging the entire skin-stiffener.

Model 2: *Landing gear of aircraft*

As stated above, non-destructive testing should be used at every stage of monitoring the manufacturing process, as well as, selection process and evaluation process. The landing gear is often referred to as the undercarriage and is a structure that is under great pressure during takeoff and landing [59,74]. To demonstrate the feasibility of the XACT internal defects detection capability, a simulation was performed using a 15-inch diameter landing gear cylinder. Figure 3.8 shows the model of landing gear where the cylinder is constructed from titanium. Defects ranging in size from 500 μm to 1000 μm are scattered in many locations at the center of a cylinder of the landing gear. Figure 3.15 illustrates the setup for the simulation, showing the embedded defects. To detect defects scattered inside the landing gear cylinder, X-ray energy and ultrasound frequencies need to penetrate 38.1 cm deep.

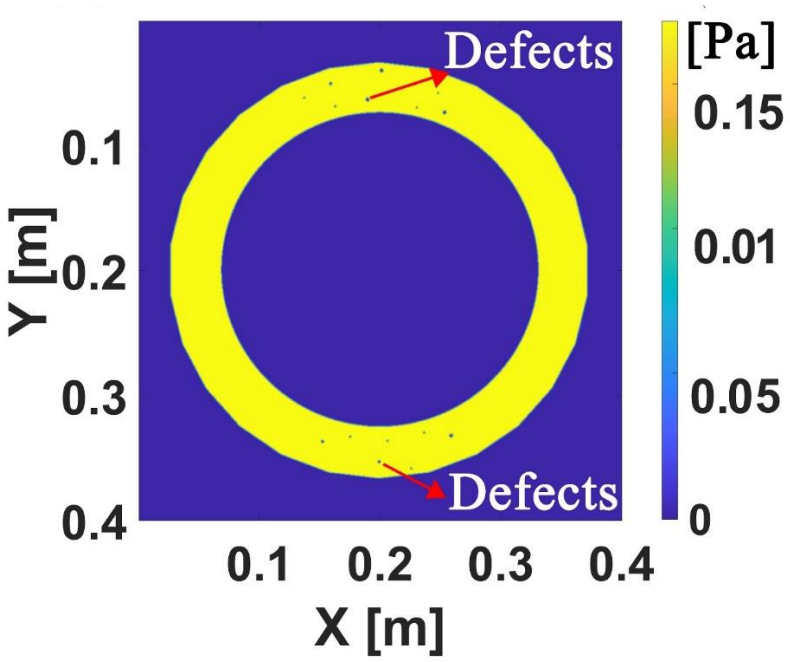

Figure 3.15. The model of simulation setup for the cylinder of the aircraft landing gear. Red dots indicate the ultrasound ring array.

In this simulation, an effective X-ray energy and ultrasound detectors of 100 KeV and 20 kHz can penetrate approximately 344 to 390 mm deep, respectively. Figure 3.16(a) shows the increase of the initial XA pressure with a linear X-ray beam with a width of 15 cm. A circular array of the transducer has a total of 256 elements that are equally spaced around the cylinder of the landing gear. To ensure a 381 mm imaging depth, the ultrasonic transducer has a center frequency of 20 kHz and 100% bandwidth.

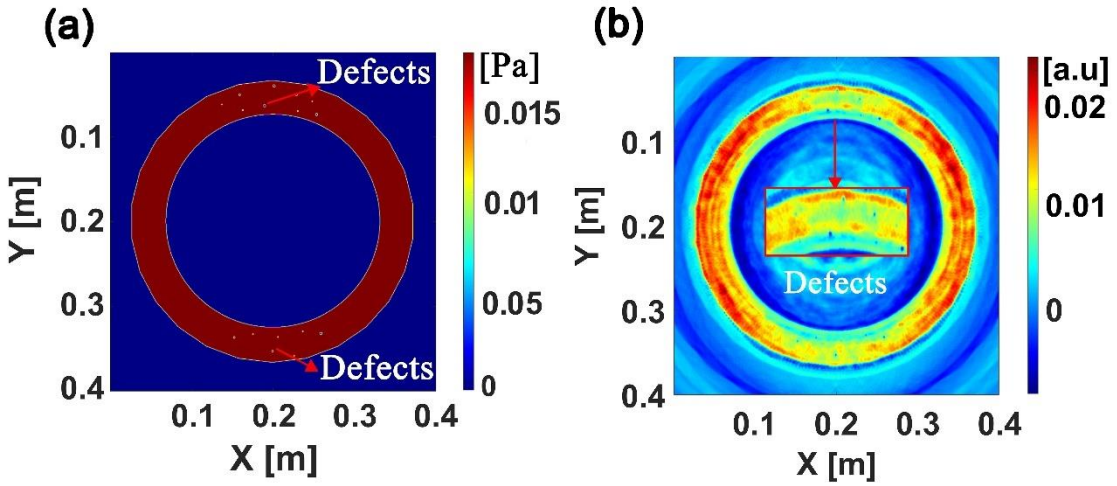

Figure 3.16. Defect detection and localization in the cylinder of landing gear using XACT (a) Initial XA pressure rise in the model with the red arrows indicate locations of defects and (b) reconstructed XACT image. A zoomed view of the defects in the red dashed rectangular.

Figure 3.16(b) shows a reconstructed XACT image from the collected XA waves. The X-ray intensity decays exponentially of penetration in this model due to the XA pressure is proportional to the X-ray fluence. However, the defects arranged within 381 mm deep are still visible. Due to the limited bandwidth, the defects often have slightly blurred edges. Which in turn, makes the location of the defects appear slightly off compared to initial defects placement. We observed that an artifact occurred from a circular array transducer. An artifact is a defect in the imaging process that causes obscurities in the reconstructed XACT image. It also often results from the properties of the material and its interactions

with a magnetic field. To remove the artifacts in images, the easiest and efficient approach through the process of elimination. A simulation without an object using the same parameter and the same setting, then using second reconstructed XACT images with a value of 0.6 subtracted the first reconstructed XACT images to remove the artifact.

Model 3: *Aircraft Fuselage Panels with Rivet*

To demonstrate the XACT defect detection capability within multi-layer metal structures, as well as, complex defects shapes. A model with intergranular corrosion was used in this simulation in Figure 3.9. Intergranular corrosion is the form of corrosion at the boundaries of the crystalline particles of a material to be more corrosive than their interior. This type of corrosion is very difficult to detect, and it will significantly weaken the adhesion force between metal plates and can severely compromise the safety of the aircraft structure [75–77]. In aircraft construction, pure metals are often unsuitable for use with rivet joints because aluminum materials often do not tolerate heat. Therefore, aluminum and stainless steel materials will be used in this demonstration due to their susceptibility to intergranular corrosion [91]. The model has two Aluminum base plates with 25.4 mm by 4mm secured by a Stainless-Steel rivet in Figure 3.9.

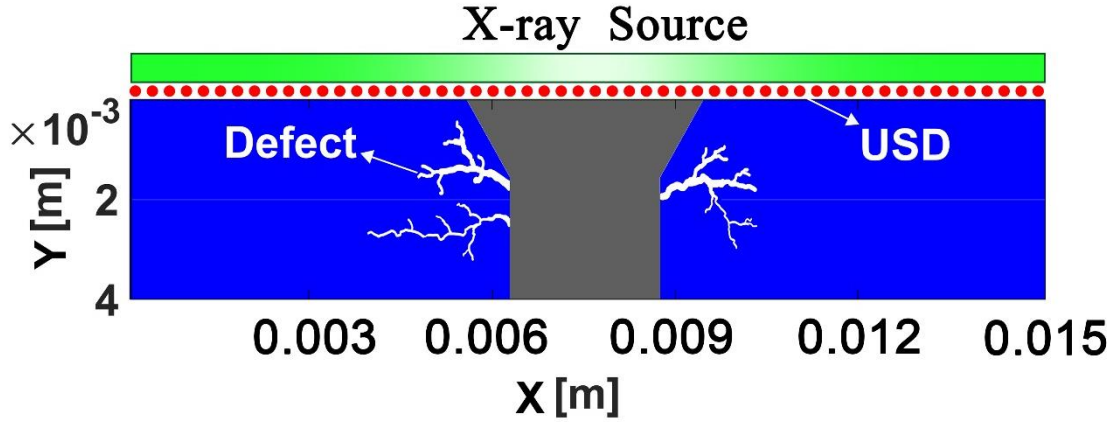

Figure 3.17. The model for the single aircraft fuselage panels with rivet with a dimension of 15 mm by 4 mm for the simulation is displayed. Red dots indicate the linear ultrasound array.

Figure 3.17 illustrates the setup for the simulation. In this model, to ensure penetration through multilayer materials with different densities, an ultrasound transducer with a center frequency of 2.5 MHz and 100% bandwidth was used to collect XA waves. A linear X-ray with an effective energy of 40 KeV is used to generate the XA waves. Figure 3.18(a) shows an increase in pressure from internal defects within the structure with the energy of 40 KeV. In this model, a linear array transducer is used to reconstruct the image with a center frequency of 2.5 MHz at 100% bandwidth. Figure 3.18(b) shows a reconstructed XACT image with strong intensity at defects. In this model, selected X-ray energy and ultrasound frequency can penetrate to 9 mm deep. A total of 150 ultrasound detectors are equally spaced on the surface of the model and the ultrasound array was slightly wider than the area with defects for good reconstruction image.

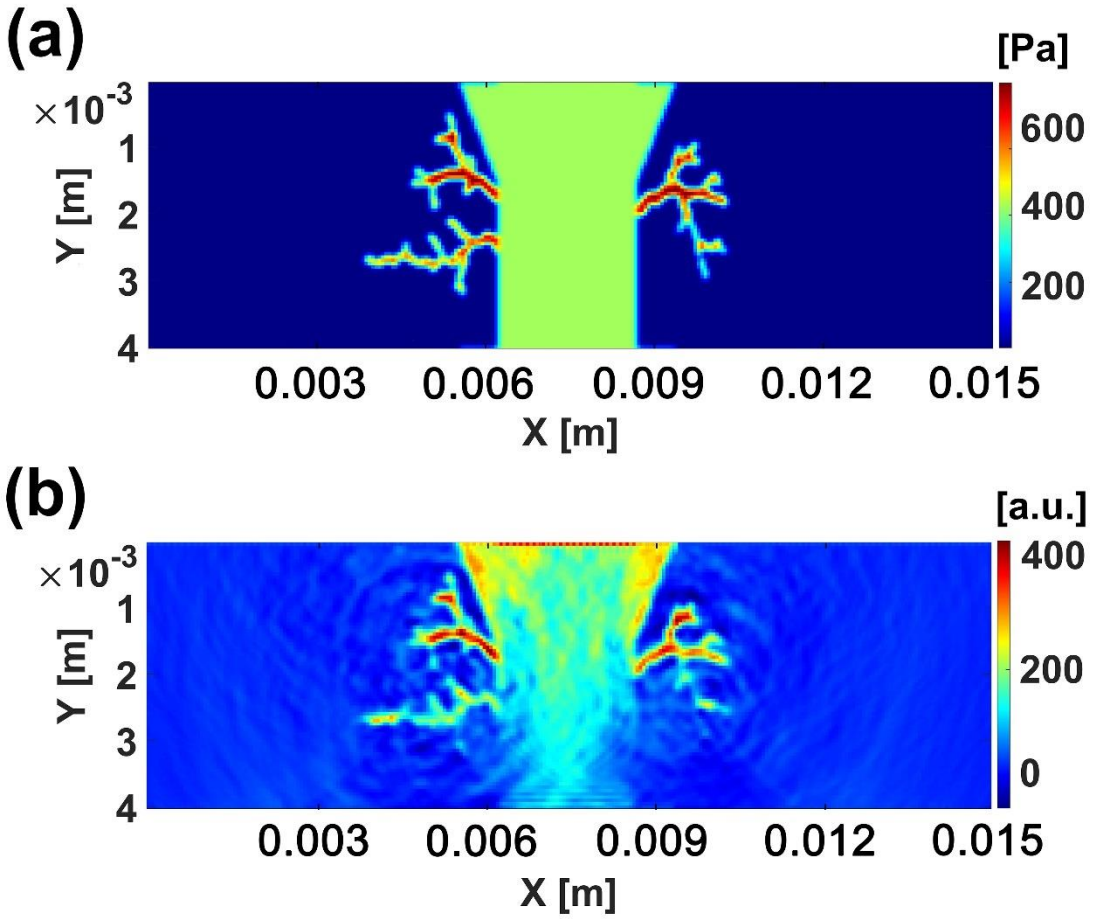

Figure 3.18. Intergranular corrosion detection and localization in Aluminum panels using XACT. (a) Initial XA pressure rise in the model. (b) a reconstructed XACT image of the aircraft fuselage panels with rivet and the defect.

Chapter 4: Discussion and Future Works

4.1 Discussion

Since the XA signal is directly proportional to the X-ray energy absorption coefficient of the penetration of the object. XACT technique can offer high imaging contrast and spatial resolution at a particular depth while maintaining the sensitivity to detect defects with a single side projection. In the first part demonstration of XACT concept, we detect the weaker XA signals, but the signals in experiments will be much stronger as we can increase the energy of the X-ray source.

In NDT imaging methods including the XACT technique, there is a trade-off between spatial resolution and penetration depth. However, the XACT technique takes advantage of the high absorption contrast from the X-ray and the spatial resolution with increasing depth compared to conventional ultrasound, as XA waves only travel in half the distance. In addition, XACT imaging is capable to detect defects in large scale structures such as aircrafts models in Figures 3.7 to 3.9, avoid two-sided accessibility of the object compared to conventional X-ray methods. These advantages make the XACT technique ideal in the NDT industry for various applications.

In these simulation studies, we observed that the acoustic impedance of metallic materials can make it fairly challenging to reconstruct XACT images. In heterogeneous aircraft structures, when the ultrasonic beam is transmitted to the mediums with different acoustic impedance, the reflection coefficient is the result of the acoustic impedance mismatch. The acoustic impedance mismatch occurs when sound propagates through materials with different densities and speeds of sound. The propagation of sound depends on the medium

in which it travels. Figure 3.18 we were able to demonstrate the XACT detection capability for three different materials through 2D simulation.

4.2 Future Works

Firstly, XACT is capable to reconstruct 3D images with a single side projection along with a planar array transducer. A 3D simulation study needs to be performed to truly demonstrate the XACT defect detection capability since XA waves propagate in all directions. However, many factors need to be carefully considered due to the acoustic impedance mismatch and sudden changes in variables that can cause poor XACT images. The difference in the density and speed of sound of a medium can create instability and crash in 3D simulations. However, the sudden changes in variables can be fixed by applying a smooth filter numerous times to stabilize the simulation.

Second, the results obtained from the simulation studies show the promising potential of the XACT technique to be implemented as an NDT system for aviation maintenance and inspections. However, to develop XACT images into a formal system, various experiments need to be done to be verified with theoretical results.

Last, we observed that an artifact occurred whenever a circular array transducer is used, while the steps used to remove artifacts. However, an algorithm or technique needs to be developed to remove artifacts more efficiently.

4.3 Conclusion

This work demonstrates the feasibility of using the new imaging modality of XACT as a method for non-destructive testing in the aviation industry and possibly to other various applications. To achieve this, a process from concept proofing to simulations is performed

with calculated parameters. This research will likely provide the basis for future research involving the use of XACT as defects detection within metallic structures.

In summary, early defect detection is critical to the safety of each flight and in various transportation systems. Currently, the XACT technique is primarily used in research laboratories, but it has the potential to be implemented in-field NDT. It is hoped that XACT technology will be adopted as a non-destructive method to improve aircraft maintenance and the inspection process in the future.

References

[1] A. Wronkowicz-Katunin, "A Brief Review on NDT&E Methods For Structural Aircraft Components," *Fatigue of Aircraft Structures*, vol. 2018, no. 10, pp. 73–81, Dec. 2018, doi: 10.2478/fas-2018-0007.

[2] S. K. Dwivedi, M. Vishwakarma, and Prof. A. Soni, "Advances and Researches on Non Destructive Testing: A Review," *Materials Today: Proceedings*, vol. 5, no. 2, Part 1, pp. 3690–3698, Jan. 2018, doi: 10.1016/j.matpr.2017.11.620.

[3] A. Beattie, L. Dahlke, and J. Gieske, "Emerging nondestructive inspection methods for aging aircraft," Jan. 1994.

[4] B. Raj, T. Jayakumar, and B. P. C. Rao, "Non-destructive testing and evaluation for structural integrity," *Sadhana*, vol. 20, no. 1, pp. 5–38, Feb. 1995, doi: 10.1007/BF02747282.

[5] A. G. Smith, "Non-destructive testing in industry aviation," *Non-Destructive Testing*, vol. 5, no. 3, pp. 170–174, Jun. 1972, doi: 10.1016/0029-1021(72)90036-9.

[6] A. Mahoon, "The role of non-destructive testing in the airworthiness certification of civil aircraft composite structures," *Composites*, vol. 19, no. 3, pp. 229–235, May 1988, doi: 10.1016/0010-4361(88)90241-8.

[7] S. Wang, J. Echeverry, L. Trevisi, K. Prather, L. Xiang, and Y. Liu, "Ultrahigh Resolution Pulsed Laser-Induced Photoacoustic Detection of Multi-Scale Damage in CFRP Composites," *Applied Sciences*, vol. 10, no. 6, Art. no. 6, Jan. 2020, doi: 10.3390/app10062106.

[8] L. W. Koester, H. Taheri, T. A. Bigelow, P. C. Collins, and L. J. Bond, "Nondestructive Testing for Metal Parts Fabricated Using Powder-Based Additive Manufacturing," *MATERIALS EVALUATION*, p. 12, 2018.

[9] H. Taheri, "Nondestructive evaluation and in-situ monitoring for metal additive manufacturing," p. 162.

[10] A. Lopez, R. Bacelar, I. Pires, T. G. Santos, J. P. Sousa, and L. Quintino, "Non-destructive testing application of radiography and ultrasound for wire and arc additive manufacturing," *Additive Manufacturing*, vol. 21, pp. 298–306, May 2018, doi: 10.1016/j.addma.2018.03.020.

[11] S. Gholizadeh, "A review of non-destructive testing methods of composite materials," *Procedia Structural Integrity*, vol. 1, 2016, Accessed: Jun. 02, 2020. [Online]. Available: https://cyberleninka.org/article/n/593997.

[12] P. Samsonov, "Nondestructive visual inspection of aging aircraft," Oakland, CA, Jul. 1995, pp. 190–196, doi: 10.1117/12.213533.

[13] X. Sun, J. Gu, S. Tang, and J. Li, "Research Progress of Visual Inspection Technology of Steel Products—A Review," *Applied Sciences*, vol. 8, no. 11, Art. no. 11, Nov. 2018, doi: 10.3390/app8112195.

[14] Yu. A. Glazkov, "Evaluation of material quality for liquid-penetrant inspection based on the visibility of the indicator patterns of flaws," *Russ J Nondestruct Test*, vol. 48, no. 4, pp. 208–217, Apr. 2012, doi: 10.1134/S1061830912040067.

[15] D. Popescu, D. Anania, C. E. Cotet, and C. G. Amza, "Fully-Automated Liquid Penetrant Inspection Line Simulation Model for Increasing Productivity," *International Journal of Simulation Modelling*, vol. 12, pp. 82–93, Jun. 2013, doi: 10.2507/IJSIMM12(2)2.225.

[16] I. Journal, R. C, and C. C. Roshan, “Non-destructive testing by liquid penetrant testing and ultrasonic testing -A review,” *INTERNATIONAL JOURNAL OF ADVANCE RESEARCH, IDEAS AND INNOVATIONS IN TECHNOLOGY*, Accessed: Jun. 02, 2020. [Online]. Available: https://www.academia.edu/39039140/Non-destructive_testing_by_liquid_penetrant_testing_and_ultrasonic_testing_-A_review.

[17] C. C. Roshan, R. C, H. V. Ram, S. K. P, and J. Solomon, “Non-destructive testing by liquid penetrant testing and ultrasonic testing – A review,” *International Journal of Advance Research, Ideas and Innovations in Technology*, vol. 5, no. 2, pp. 694–697, Mar. 2019, doi: XX.XXX/IJARIIT-V5I2-1529.

[18] A. Zolfaghari and F. Kolahan, “Reliability and sensitivity of visible liquid penetrant NDT for inspection of welded components,” *Materials Testing*, vol. 59, pp. 290–294, Mar. 2017, doi: 10.3139/120.111000.

[19] “Review Paper: Non-destructive testing by liquid penetrant testing and ultrasonic testing – A review - published by C. Chris Roshan in IJARIIT Journal.” https://www.ijariit.com/manuscript/non-destructive-testing-by-liquid-penetrant-testing-and-ultrasonic-testing-a-review/ (accessed Jun. 02, 2020).

[20] “(PDF) Eddy Current Testing: Basics,” *ResearchGate*. https://www.researchgate.net/publication/258935465_Eddy_Current_Testing_Basics (accessed Jun. 02, 2020).

[21] J. García-Martín, J. Gómez-Gil, and E. Vázquez-Sánchez, “Non-Destructive Techniques Based on Eddy Current Testing,” *Sensors*, vol. 11, no. 3, pp. 2525–2565, Feb. 2011, doi: 10.3390/s110302525.

[22] A. N. AbdAlla, M. A. Faraj, F. Samsuri, D. Rifai, K. Ali, and Y. Al-Douri, “Challenges in improving the performance of eddy current testing: Review,” *Measurement and Control*, vol. 52, no. 1–2, pp. 46–64, Jan. 2019, doi: 10.1177/0020294018801382.

[23] J. Bowler and N. Bowler, “Evaluation of the magnetic field near a crack with application to magnetic particle inspection,” *Journal of Physics D: Applied Physics*, vol. 35, p. 2237, Sep. 2002, doi: 10.1088/0022-3727/35/18/301.

[24] Z. Cai, D. Zou, and C. Liu, “Research on Eddy-Current Testing of Functional Polymer Composite Material,” *IEEE Transactions on Magnetics*, vol. 54, no. 11, pp. 1–5, Nov. 2018, doi: 10.1109/TMAG.2018.2832467.

[25] D. C. Jiles, “Review of magnetic methods for nondestructive evaluation (Part 2),” *NDT International*, vol. 23, no. 2, pp. 83–92, Apr. 1990, doi: 10.1016/0308-9126(90)91892-W.

[26] W. G. King, “A practical introduction to magnetic particle testing: Basic rules for satisfactory detection,” *Non-Destructive Testing*, vol. 1, no. 2, pp. 84–90, Nov. 1967, doi: 10.1016/0029-1021(67)90027-8.

[27] C. Chircov, A. M. Grumezescu, and A. M. Holban, “Magnetic Particles for Advanced Molecular Diagnosis,” *Materials (Basel)*, vol. 12, no. 13, Jul. 2019, doi: 10.3390/ma12132158.

[28] A. Anoshkin, V. Osokin, A. Tretyakov, N. Potrakhov, and V. Bessonov, “Application of operational radiographic inspection method for flaw detection of blade straightener from polymeric composite materials,” *Journal of Physics:*

Conference Series, vol. 808, p. 012003, Feb. 2017, doi: 10.1088/1742-6596/808/1/012003.
[29] D. Kanzler, U. Ewert, C. Müller, and J. Pitkänen, "Observer POD for radiographic testing," *AIP Conference Proceedings*, vol. 1650, no. 1, pp. 562–570, Mar. 2015, doi: 10.1063/1.4914654.
[30] E. Taha, M. S. Mohammed, and E. Banoqitah, "Radiographic Nondestructive Testing Simulations Using gate Software Toolkit," *ASME J of Nuclear Rad Sci*, vol. 6, no. 1, Jan. 2020, doi: 10.1115/1.4044909.
[31] E. Taha, M. Siddig, and E. Banoqitah, "Radiographic Testing Simulations for NDT Research, Education, and Training," *Journal of Nuclear Engineering and Radiation Science*, vol. 6, Sep. 2019, doi: 10.1115/1.4044909.
[32] M. Anwar, M. Y. Ahmed, M. Riyaaz, S. Siddiqui, and S. A. Pasha, "Testing by Radiography on Welded Mild Steel (NDT Method)," vol. 3, no. 08, p. 5.
[33] T. Zavadil, "Nondestructive Testing Ultrasonic Technique for Localization of Areas Subjected to Creep Deformation on In-Service Pipings Manufactured From Low-Alloyed Steel," *J. Pressure Vessel Technol*, vol. 141, no. 6, Dec. 2019, doi: 10.1115/1.4043998.
[34] A. Katunin, A. Wronkowicz-Katunin, and K. Dragan, "Impact Damage Evaluation in Composite Structures Based on Fusion of Results of Ultrasonic Testing and X-ray Computed Tomography," *Sensors*, vol. 20, no. 7, Art. no. 7, Jan. 2020, doi: 10.3390/s20071867.
[35] M. G. Lozev, R. L. Spencer, and D. Hodgkinson, "Optimized Inspection of Thin-Walled Pipe Welds Using Advanced Ultrasonic Techniques," *J. Pressure Vessel Technol*, vol. 127, no. 3, pp. 237–243, Aug. 2005, doi: 10.1115/1.1991876.
[36] H. Tyrer and D. C. Hollamby, "Ultrasonic flaw detection in the aircraft industry: Aspects of technique and standardization," *Ultrasonics*, vol. 1, no. 4, pp. 211–219, Oct. 1963, doi: 10.1016/0041-624X(63)90169-0.
[37] A. Sharma and A. Sinha, "Ultrasonic Testing for Mechanical Engineering Domain: Present and Future Perspective," Nov. 2018. doi: 10.22105/riej.2018.100730.1018.
[38] S. Gao, C. Baker, W. Cai, L. Chen, and X. Bao, "10 kHz-34 MHz ultrasound detection based on a dual-core hybrid taper," *APL Photonics*, vol. 4, no. 11, p. 110805, Nov. 2019, doi: 10.1063/1.5093987.
[39] J. P. Lynch and K. J. Loh, "A summary review of wireless sensors and sensor networks for structural health monitoring," *The Shock and Vibration Digest*, vol. 38, no. 2, pp. 91–130, Mar. 2006.
[40] J. Ou and H. Li, "Structural Health Monitoring in mainland China: Review and Future Trends," *Structural Health Monitoring*, vol. 9, no. 3, pp. 219–231, May 2010, doi: 10.1177/1475921710365269.
[41] Y. Liu and S. Nayak, "Structural Health Monitoring: State of the Art and Perspectives," *JOM*, vol. 64, no. 7, pp. 789–792, Jul. 2012, doi: 10.1007/s11837-012-0370-9.
[42] S. Abbas, F. Li, and J. Qiu, "A Review on SHM Techniques and Current Challenges for Characteristic Investigation of Damage in Composite Material Components of Aviation Industry," *MPC*, vol. 7, no. 1, pp. 224–258, Jun. 2018, doi: 10.1520/MPC20170167.

[43] Y. Liu, M. Y. Fard, A. Chattopadhyay, and D. Doyle, “Damage assessment of CFRP composites using a time–frequency approach:,” *Journal of Intelligent Material Systems and Structures*, Jan. 2012, doi: 10.1177/1045389X11434171.
[44] H. Zhang, R. Yang, Y. He, A. Foudazi, L. Cheng, and G. Tian, “A Review of Microwave Thermography Nondestructive Testing and Evaluation,” *Sensors*, vol. 17, no. 5, Art. no. 5, May 2017, doi: 10.3390/s17051123.
[45] Y. Liu, S. B. Kim, A. Chattopadhyay, and D. Doyle, “Application of System-Identification Techniquest to Health Monitoring of On-Orbit Satellite Boom Structures,” *Journal of Spacecraft and Rockets*, vol. 48, no. 4, pp. 589–598, 2011, doi: 10.2514/1.51818.
[46] S. S. Kulkarni and J. D. Achenbach, “Structural Health Monitoring and Damage Prognosis in Fatigue:,” *Structural Health Monitoring*, Mar. 2008, doi: 10.1177/1475921707081973.
[47] Y. Liu, S. Mohanty, and A. Chattopadhyay, “Condition based structural health monitoring and prognosis of composite structures under uniaxial and biaxial loading,” *Journal of Nondestructive Evaluation*, vol. 29, no. 3, pp. 181–188, Sep. 2010, doi: 10.1007/s10921-010-0076-2.
[48] D. Mitsheal, “A Review of Structural Health Monitoring Techniques as Applied to Composite Structures,” p. 57, 2017.
[49] Y. Liu and A. Chattopadhyay, “Low-velocity impact damage monitoring of a sandwich composite wing,” *Journal of Intelligent Material Systems and Structures*, vol. 24, no. 17, pp. 2074–2083, Nov. 2013, doi: 10.1177/1045389X12453964.
[50] D. Feng and M. Q. Feng, “Computer vision for SHM of civil infrastructure: From dynamic response measurement to damage detection – A review,” *Engineering Structures*, vol. 156, pp. 105–117, Feb. 2018, doi: 10.1016/j.engstruct.2017.11.018.
[51] G. W. O. Howe, “Alexander Graham Bell and the Invention of the Telephone*,” *Nature*, vol. 159, no. 4040, Art. no. 4040, Apr. 1947, doi: 10.1038/159455a0.
[52] K. Y. Kim and W. Sachse, “X-ray generated ultrasound,” *Appl. Phys. Lett.*, vol. 43, no. 12, pp. 1099–1101, Dec. 1983, doi: 10.1063/1.94240.
[53] T. Bowen, C. X. Chen, S. C. Liew, W. R. Lutz, and R. L. Nasoni, “Observation of ultrasonic emission from edges of therapeutic X-ray beams,” *Phys. Med. Biol.*, vol. 36, no. 4, pp. 537–539, Apr. 1991, doi: 10.1088/0031-9155/36/4/011.
[54] L. Xiang, B. Han, C. Carpenter, G. Pratx, Y. Kuang, and L. Xing, “X-ray acoustic computed tomography with pulsed x-ray beam from a medical linear accelerator,” *Medical Physics*, vol. 40, no. 1, p. 010701, 2013, doi: 10.1118/1.4771935.
[55] L. Xiang, B. Han, C. Carpenter, G. Pratx, Y. Kuang, and L. Xing, “X-ray induced photoacoustic tomography,” in *Photons Plus Ultrasound: Imaging and Sensing 2013*, Mar. 2013, vol. 8581, p. 85811I, doi: 10.1117/12.2005765.
[56] L. Xiang *et al.*, “TH-A-141-02: X-Ray Acoustic Computed Tomography: Concept and Design,” *Medical Physics*, vol. 40, no. 6Part31, pp. 522–522, 2013, doi: 10.1118/1.4815707.
[57] L. Xiang, M. Ahmad, A. Nikoozadeh, G. Pratx, B. Khuri-Yakub, and L. Xing, “TU-A-9A-07: X-Ray Acoustic Computed Tomography (XACT): 100% Sensitivity to X-Ray Absorption,” *Medical Physics*, vol. 41, no. 6Part26, pp. 448–448, 2014, doi: 10.1118/1.4889242.

[58] S. Hickling, H. Lei, M. Hobson, P. Léger, X. Wang, and I. E. Naqa, "Experimental evaluation of x-ray acoustic computed tomography for radiotherapy dosimetry applications," *Medical Physics*, vol. 44, no. 2, pp. 608–617, 2017, doi: 10.1002/mp.12039.
[59] S. Hickling, M. Hobson, and I. E. Naqa, "Feasibility of X-Ray Acoustic Computed Tomography as a Tool for Noninvasive Volumetric In Vivo Dosimetry," *International Journal of Radiation Oncology, Biology, Physics*, vol. 90, no. 1, p. S843, Sep. 2014, doi: 10.1016/j.ijrobp.2014.05.2417.
[60] S. Hickling, H. Lei, M. Hobson, P. Leger, X. Wang, and I. E. Naqa, "Sci-Thur AM: YIS – 02: Imaging dose distributions through the detection of radiation-induced acoustic waves," *Medical Physics*, vol. 43, no. 8Part2, pp. 4928–4928, 2016, doi: 10.1118/1.4961751.
[61] S. Tang, C. Ramseyer, P. Samant, and L. Xiang, "X-ray-induced acoustic computed tomography of concrete infrastructure," *Appl. Phys. Lett.*, vol. 112, no. 6, p. 063504, Feb. 2018, doi: 10.1063/1.5009936.
[62] Y. Fang, A. N. Vasil'ev, and V. V. Mikhailin, "Theory of X-ray photoacoustic spectroscopy," *Appl. Phys. A*, vol. 60, no. 3, pp. 333–341, Mar. 1995, doi: 10.1007/BF01538414.
[63] L. V. Wang, "Tutorial on Photoacoustic Microscopy and Computed Tomography," *IEEE Journal of Selected Topics in Quantum Electronics*, vol. 14, no. 1, pp. 171–179, Jan. 2008, doi: 10.1109/JSTQE.2007.913398.
[64] M. E. Garcia, G. M. Pastor, and K. H. Bennemann, "Theory for the Photoacoustic Response to X-Ray Absorption," *Phys. Rev. Lett.*, vol. 61, no. 1, pp. 121–124, Jul. 1988, doi: 10.1103/PhysRevLett.61.121.
[65] J. Xia, J. Yao, and L. V. Wang, "Photoacoustic tomography: principles and advances," *Electromagn Waves (Camb)*, vol. 147, pp. 1–22, 2014.
[66] S. Liu, R. Zhang, Z. Zheng, and Y. Zheng, "Electromagnetic–Acoustic Sensing for Biomedical Applications," *Sensors (Basel)*, vol. 18, no. 10, Sep. 2018, doi: 10.3390/s18103203.
[67] S. Tang *et al.*, "X-ray-induced acoustic computed tomography with an ultrasound transducer ring-array," *Appl. Phys. Lett.*, vol. 110, no. 10, p. 103504, Mar. 2017, doi: 10.1063/1.4978049.
[68] R. Baskar, K. A. Lee, R. Yeo, and K.-W. Yeoh, "Cancer and Radiation Therapy: Current Advances and Future Directions," *Int J Med Sci*, vol. 9, no. 3, pp. 193–199, Feb. 2012, doi: 10.7150/ijms.3635.
[69] J. Malicki, "Medical physics in radiotherapy: The importance of preserving clinical responsibilities and expanding the profession's role in research, education, and quality control," *Rep Pract Oncol Radiother*, vol. 20, no. 3, pp. 161–169, 2015, doi: 10.1016/j.rpor.2015.01.001.
[70] "Chapter 17. Class D Airspace." https://tfmlearning.faa.gov/Publications/atpubs/AIR/air1701.html (accessed Jun. 14, 2020).
[71] "Non-Destructive Testing for Landing Gear Applications | SBIR.gov." https://www.sbir.gov/node/1482317 (accessed Jun. 14, 2020).

[72] Z. Li and T. Mu, “Study on Dimension of Landing Gear Bogie for Civil Aircraft,” *IOP Conference Series: Materials Science and Engineering*, vol. 563, p. 042042, Aug. 2019, doi: 10.1088/1757-899X/563/4/042042.
[73] T. Tran, P. Samant, L. Xiang, and Y. Liu, “X-Ray Induced Acoustic Computed Tomography for Non-Destructive Testing of Aircraft Structure,” presented at the ASME 2019 International Mechanical Engineering Congress and Exposition, Jan. 2020, doi: 10.1115/IMECE2019-10480.
[74] L. V. Nguyen and L. A. Kunyansky, “A Dissipative Time Reversal Technique for Photoacoustic Tomography in a Cavity,” *SIAM J. Imaging Sciences*, 2016, doi: 10.1137/15M1049683.
[75] E. Bossy *et al.*, “Time reversal of photoacoustic waves,” *Appl. Phys. Lett.*, vol. 89, no. 18, p. 184108, Oct. 2006, doi: 10.1063/1.2382732.
[76] M. Sun, Z. Wu, T. Liu, J. Hu, G. Wu, and N. Feng, “Time Reversal Reconstruction Algorithm Based on PSO Optimized SVM Interpolation for Photoacoustic Imaging,” *Mathematical Problems in Engineering*, May 03, 2015. https://www.hindawi.com/journals/mpe/2015/795092/ (accessed Jun. 02, 2020).
[77] B. E. Treeby and B. T. Cox, “k-Wave: MATLAB toolbox for the simulation and reconstruction of photoacoustic wave fields,” *JBO*, vol. 15, no. 2, p. 021314, Mar. 2010, doi: 10.1117/1.3360308.
[78] B. E. Treeby, J. Jaros, D. Rohrbach, and B. T. Cox, “Modelling elastic wave propagation using the k-Wave MATLAB Toolbox,” in *2014 IEEE International Ultrasonics Symposium*, Sep. 2014, pp. 146–149, doi: 10.1109/ULTSYM.2014.0037.
[79] “Photoacoustic Imaging and Spectroscopy,” *CRC Press*. https://www.routledge.com/Photoacoustic-Imaging-and-Spectroscopy/Wang/p/book/9781420059915 (accessed Jun. 02, 2020).
[80] M. Xu and L. V. Wang, “Photoacoustic imaging in biomedicine,” *Review of Scientific Instruments*, vol. 77, no. 4, p. 041101, Apr. 2006, doi: 10.1063/1.2195024.
[81] P. Beard, “Biomedical photoacoustic imaging,” *Interface Focus*, vol. 1, no. 4, pp. 602–631, Aug. 2011, doi: 10.1098/rsfs.2011.0028.
[82] “Applied Sciences | Free Full-Text | A Comprehensive Report on Ultrasonic Attenuation of Engineering Materials, Including Metals, Ceramics, Polymers, Fiber-Reinforced Composites, Wood, and Rocks | HTML.” https://www.mdpi.com/2076-3417/10/7/2230/htm (accessed Jun. 14, 2020).
[83] R. KLINMAN and E. T. STEPHENSON, “Ultrasonic prediction of grain size and mechanical properties on plain carbon steel,” *Mater. eval*, vol. 39, no. 12, pp. 1116–1120, 1981.
[84] “Ultrasonic prediction of grain size and mechanical properties on plain carbon steel - Search results - Pascal and Francis Bibliographic Databases.” https://pascal-francis.inist.fr/vibad/index.php?action=getRecordDetail&idt=8997874 (accessed Jun. 14, 2020).
[85] T. H. G. Megson, “CHAPTER 11 - Structural Components of Aircraft,” in *Introduction to Aircraft Structural Analysis*, T. H. G. Megson, Ed. Boston: Butterworth-Heinemann, 2010, pp. 351–371.

[86] T. H. G. Megson, “Chapter 23 - Fuselage frames and wing ribs,” in *Introduction to Aircraft Structural Analysis (Third Edition)*, T. H. G. Megson, Ed. Butterworth-Heinemann, 2018, pp. 673–684.
[87] A. Dubey, S. Gupta, B. Bodramoni, and V. Undavalli, “Landing Gear of an Aircraft Structure: A Review,” *International Journal of Engineering Research and Technology*, vol. 4, p. 20, Dec. 2015, doi: 10.17577/IJERTV4IS120005.
[88] A. A. Johnson and R. J. Storey, “Intergranular corrosion of a light aircraft aluminum alloy propeller,” *J Fail. Anal. and Preven.*, vol. 4, no. 6, pp. 19–22, Dec. 2004, doi: 10.1361/15477020421809.
[89] S. P. Knight, M. Salagaras, and A. R. Trueman, “The study of intergranular corrosion in aircraft aluminium alloys using X-ray tomography,” *Corrosion Science*, vol. 53, no. 2, pp. 727–734, Feb. 2011, doi: 10.1016/j.corsci.2010.11.005.
[90] M. Czaban, “Aircraft corrosion - Review of corrosion processes and its effects in selected cases,” *Fatigue of Aircraft Structures*, May 2019, doi: 10.2478/FAS-2018-0001.
[91] S. Kadry, “Corrosion analysis of stainless steel,” *European Journal of Scientific Research*, vol. 22, pp. 508–516, Jan. 2008.